https://doi.org/10.5194/bg-2020-333
Preprint. Discussion started: 5 November 2020

Biogeosciences Discussions
Open Access
EGU

Archaeal Intact Polar Lipids in Polar Waters: A Comparison Between the Amundsen and Scotia Seas

Charlotte L. Spencer-Jones[1], Erin L. McClymont[1], Nicole J. Bale[2], Ellen C. Hopmans[2], Stefan Schouten[2,3], Juliane Müller[4], E. Povl Abrahamsen[5], Claire Allen[5], Torsten Bickert[4], Claus-Dieter Hillenbrand[5], Elaine Mawbey[5], Victoria Peck[5], Aleksandra Svalova[6], James A. Smith[5]

[1]Department of Geography, Durham University, Lower Mountjoy, South Road, Durham, DH1 3LE, UK.
[2]NIOZ Royal Netherlands Institute for Sea Research, Department of Marine Microbiology and Biogeochemistry, P.O. Box 59, 1790 AB Den Burg, Texel, The Netherlands.
[3] Department of Earth Sciences, Utrecht University, Utrecht, The Netherlands.
[4]Alfred Wegener Institute, Helmholtz Center for Polar and Marine Research, 27568 Bremerhaven, Germany.
[5]British Antarctic Survey, High Cross, Madingley Road, Cambridge, CB3 0ET, UK.
[6] School of Natural and Environmental Sciences, Newcastle University, Newcastle-upon-Tyne, NE1 7RU, UK.

Correspondence to: Charlotte L. Spencer-Jones (charlotte.spencer-jones@open.ac.uk)

Abstract

The West Antarctic Ice Sheet (WAIS) is one of the largest potential sources of future sea-level rise, with glaciers draining the WAIS thinning at an accelerating rate over the past 40 years. Due to difficulties in calibrating palaeoceanographic proxies for the Southern Ocean, it remains difficult to assess whether similar changes have occurred earlier during the Holocene or whether there is underlying centennial to millennial scale forcing in oceanic variability. Archaeal lipid – based proxies, specifically Glycerol Dialkyl Glycerol Tetraether (GDGT) (e.g. TEX_{86} and TEX_{86}^{L}) are powerful tools for reconstructing ocean temperature, but these proxies have been shown previously to be difficult to apply to the Southern Ocean. A greater understanding of the parameters that control Southern Ocean GDGT distributions would improve the application of these biomarker proxies and thus help provide a longer-term perspective on ocean forcing of Antarctic ice sheet changes. In this study, we characterised intact polar lipid (IPL) - GDGTs, representing (recently) living archaeal population in suspended particulate matter from the Amundsen Sea and the Scotia Sea. Shifts in IPL-GDGT signatures across well-defined fronts of the Southern Ocean revealed a correlation between the physicochemical parameters of these water masses and IPL-GDGT distributions. Further analysis is required to elucidate the additional role of productivity and nutrient availability on Southern Ocean IPL-GDGT distributions. Of particular note for proxy development in the Amundsen Sea is that IPL-

https://doi.org/10.5194/bg-2020-333
Preprint. Discussion started: 5 November 2020


Biogeosciences Discussions Open Access EGU

GDGTs are likely actively synthesised at Circumpolar Deep Water depths and may be a significant source of GDGTs exported to the sedimentary record in this region.

Key words

Southern Ocean, Intact Polar Lipid (IPL), Glycerol Dialkyl Glycerol Tetraether (GDGT), Amundsen Sea, Scotia Sea, Circumpolar Deep Water, Archaea, Thaumarchaeota.

1. Introduction

Over the past ca. 50 years the West Antarctic Ice Sheet (WAIS) has lost ice mass at an accelerating rate with some suggesting that the complete collapse of the WAIS may already be underway (Joughin et al., 2014; Mouginot et al., 2014; Rignot et al., 2019). The WAIS is grounded below sea level and the edges of the ice sheet are floating ice shelves that are, highly sensitive to changes in ocean properties. Widespread ice sheet/shelf thinning will likely have influence on biogeochemical cycling through ocean productivity (Raiswell et al., 2008; Menviel et al., 2010; Wadham et al., 2013), carbon reservoirs and carbon sequestration (Yager et al., 2012; Wadham et al., 2019), in addition to sea ice and ocean circulation changes (Menivel et al., 2010).

One of the challenges in understanding and predicting the behaviour of WAIS is a lack of long-term ocean temperature records (i.e. prior to the satellite era ~1992). Such records are needed to better understand the links between WAIS stability, physical properties of the Southern Ocean, and biogeochemistry which might vary on centennial to millennial timescales (Smith et al., 2017; Hillenbrand et al., 2017). Organic geochemical proxies based on the ratios of archaeal membrane lipids can be used to reconstruct past ocean temperature and biogeochemistry. Glycerol dialkyl glycerol tetraether (GDGT) lipids are particularly promising with the TEX_{86}, TEX_{86}^{L} and OH-GDGT proxies having been widely used to reconstruct ocean temperatures in tropical, temperate, and northern polar regions (e.g. Jenkyns et al., 2004; Huguet et al., 2006, 2011; Sinninghe Damsté et al., 2010; Darfeuil et al., 2016). In contrast, only a handful of studies have successfully applied these proxies in the Southern Ocean (Kim et al., 2012; Shevenell et al., 2011; Etourneau et al., 2013, 2019). This reflects a combination of low concentrations of GDGTs as well as an incomplete understanding of archaeal populations and habitat/niche preference (Kim et al., 2010). A better understanding of the source of GDGTs in the Southern Ocean and factors that impact archaeal populations could improve application of TEX_{86} based proxies in this environment.

https://doi.org/10.5194/bg-2020-333
Preprint. Discussion started: 5 November 2020

1.1. Tracing Archaea with Intact Polar Lipids

Archaea are a key component of picoplankton within the polar oceans (Delong et al., 1994; Murray et al., 1998; Church et al., 2003; Kirchman et al., 2007; Alonso-Saez et al., 2008) and have an important role in biogeochemical cycling and in marine food webs. GDGTs are important cell membrane components present in many marine archaea (Schouten et al., 2013 and references therein) including the ammonia oxidising archaea (AOA) Thaumarchaeota (previously assigned to the phylum Crenarchaeota; Brochier-Armanet et al., 2008; Spang et al., 2010). Marine archaea produce isoprenoid GDGTs with a polar head group (intact polar lipids - IPLs). Upon cell death the polar head group is relatively rapidly cleaved off resulting in the preservation of the core GDGT lipid (c-GDGTs). c-GDGTs are subsequently preserved in the sedimentary record and can be used to reconstruct Antarctic palaeoenvironmental change over long time scales (Kim et al., 2012; Shevenell et al., 2011; Etourneau et al., 2013, 2019). Thaumarchaeota are a major source of GDGTs to the environment with pure culture studies detecting GDGTs with 0-3 cyclopentane moieties, crenarchaeol (cren, which contains 4 cyclopentane moieties and a cyclohexane moiety) and cren regio isomer (cren', Schouten et al., 2000; Sinninghe Damsté et al., 2018). Other archaeal phyla (e.g. marine Euryarchaeota group II) have been hypothesised as sources of GDGTs to the marine realm (Lincoln et al., 2014a,b), however this source is unlikely to be significant in marine samples (Schouten el. al., 2014; Zeng et al., 2019; Besseling et al., 2020). Furthermore, archaea exist throughout the marine water column with several studies suggesting a GDGT contribution to sediments from “deep water” Thaumarcheota (e.g. Ingalls et al., 2006; Shah et al., 2008; Kim et al., 2016).

IPL-GDGTs may be used as proxies for tracing (recently) living archaeal populations (e.g. Pitcher et al., 2011; Sinninghe Damsté et al., 2012; Elling et al., 2014, 2017). AOA enrichment cultures reveal three common GDGT head groups; monohexose (MH), dihexose (DH), and hexose-phosphohexose (HPH) (Schouten et al., 2008; Pitcher et al., 2010, 2011), with all three IPL head groups reported in environmental samples (Lipp et al., 2008; Lipp and Hinrichs, 2009; Schubotz et al., 2009; Schouten et al., 2012; Xie et al., 2014; Evans et al., 2017; Sollich et al., 2017; Besseling et al., 2018). HPHs are a common IPL in all AOA enrichment cultures, to date, with MH and DH intermittently present (Pitcher et al., 2011; Elling et al., 2017; Bale et al., 2019). The interpretation of IPL-GDGTs as proxies for living archaeal biomass is complicated by their degradation to c-GDGTs with increasing evidence that some IPLs are preserved following cell death

https://doi.org/10.5194/bg-2020-333
Preprint. Discussion started: 5 November 2020

(Bauersachs et al., 2010; Huguet et al., 2010; Schouten et al., 2010; Xie et al., 2013; Lengger et al., 2014). Kinetic modelling has suggested greater preservation of glycolipids compared with phospholipids (Schouten et al., 2010), therefore suggesting that HPH-GDGTs may have potential as biomarkers for living, metabolically active, Thaumarchaeotal populations (Schouten et al., 2012; Elling et al., 2014, 2017). However, HPH-GDGT abundance is variable across the 1.1a Thaumarchaeota clade which could make the interpretation of this biomarker in environmental studies complex (Elling et al., 2017). DH-GDGTs and DH-OH-GDGT on the other hand are thought to be produced exclusively by 1.1a Thaumarchaeota with more uniform abundance across the clade (Pitcher et al., 2011; Sinninghe Damsté et al., 2012), and could therefore be potential tracers for living Thaumarchaeota (Elling et al., 2017).

In this study, we present the first characterisation of IPL-GDGTs in suspended particulate matter (SPM) from two locations in the Southern Ocean, the Scotia Sea and the Amundsen Sea. The first aim of this study is to characterise the distributions of IPL-GDGTs within the Southern Ocean in order to expand our understanding of Thaumarchaeotal distributions in Polar Regions and improve our interpretation of GDGT based proxies. The second aim of this study is to understand the environmental controls on IPL-GDGT distributions in the Southern Ocean. In this study, we analyse the water column profiles of IPL-GDGTs with 18 samples from the Amundsen Sea and 15 samples from a transect in the Scotia and Weddell Sea.

1.2. Study Area

The Southern Ocean drives global thermohaline circulation and is therefore a major regulator of Earth's oceans and climate (Carter et al., 2009). The clockwise flowing Antarctic Circumpolar Current (ACC) connects all the major ocean basins resulting in a major role in the distribution of heat, salt, and gasses (Carter et al., 2009). The surface waters of the Southern Ocean show clear shifts in water properties (salinity and temperature) which mark ocean fronts, and in the present study include; Sub-Antarctic front (SAF), the Polar Front (PF), the Southern Front of the ACC (SACCF), and the Southern Boundary of the ACC (SBACC) (Carter et al., 2009 and references therein). Antarctic surface waters (AASW; 100m thick), extending from the Antarctic continental shelf to the PF, are characterised by near freezing temperatures and salinity values up to 34.3 practical salinity units (PSU), although these properties can vary on a regional basis (Carter et al., 2009 and references therein). The transition between AASW south of the PF and Sub-Antarctic surface water (SASW) north of the SAF occurs in the Polar Frontal Zone. Due to complex mixing processes,

https://doi.org/10.5194/bg-2020-333
Preprint. Discussion started: 5 November 2020

116 the properties of surface water in the Polar Frontal Zone are often variable, but this water is generally
117 warmer (3-8 °C) and less dense (salinity 34-34.4 PSU) than AASW (Carter et al., 2009 and references
118 therein). Lastly, SASW is comparatively warmer (6-12 °C) with salinity >34.3 PSU (Carter et al., 2009 and
119 references therein). Circumpolar Deep Water (CDW) together with CDW-derived, modified deep-water
120 masses, such as Warm Deep Water in the Weddell Gyre (e.g. Vernet et al., 2019) is a key Southern Ocean
121 water mass and can be detected between ~1400 m and >3500 m depth offshore from the Antarctic continent.
122 CDW can rise to meet AASW or even outcrop along the Antarctic continental margin (Carter et al., 2009 and
123 references therein). Mixing of CDW with different water masses gives rise to two types: Upper CDW
124 (UCDW) defined by an oxygen minimum, high nutrient concentrations, and a depth of 1400-2500 m; and
125 Lower CDW (LCDW) defined by a salinity maximum of 34.70-34.75 PSU (Carter et al., 2009 and
126 references therein). In contrast to UCDW, LCDW extends south of the SBACC (Orsi et al., 1995), is
127 upwelling at the continental slope, and can protrude onto the shelf where it mixes with super cooled shelf
128 waters, renewing LCDW and forming Antarctic Bottom Water (AABW) (Carter et al., 2009 and references
129 therein).
130 The Scotia Sea is located in the eastern Atlantic sector of the Southern Ocean (20°W to 65°W) bounded by
131 the South Atlantic Ocean to the North, the Drake Passage to the West, and by the Weddell Sea to the South
132 (Figure 1). The Scotia Sea is influenced by the eastward flow of the ACC, via the Drake Passage, and by a
133 northward component of the ACC, caused by topographic steering and northward outflow of recently
134 ventilated waters from the Weddell Sea , whereby Weddell Sea Deep Water (WSDW) is incorporated into
135 the ACC (Locarnini et al., 1993; Naveira Grabato et al., 2002a,b), thus creating a region of high mixing
136 (Heywood et al., 2002) and intense water mass modification (Locarnini et al., 1993).
137 The Amundsen Sea extends from 100°W to 130°W and is bounded by the Sub-Antarctic Pacific to the North
138 (Figure 1). The Amundsen Sea water column south of the PF mainly consist of a thin upper layer of cold and
139 fresh AASW overlying relatively warm CDW. The Amundsen Sea embayment is located offshore from one
140 of the major WAIS drainage basins and observations show a clear trend in glacial retreat over recent decades
141 (e.g. Mouginot et al., 2014; Paolo et al., 2015; Rignot et al., 2019). The deep ice shelves (extending up to
142 1000 m below sea level) surrounding the Amundsen Sea embayment are exposed to unmodified CDW which
143 can be up to 4 °C above the *in situ* melting point (Jacobs et al., 1996, 2011; Rignot and Jacobs, 2002; Jenkins

https://doi.org/10.5194/bg-2020-333
Preprint. Discussion started: 5 November 2020

et al., 2010; Rignot et al., 2013; Webber et al., 2017) so that CDW may drive enhanced melt rates and ice sheet instability in this region (Shepherd et al., 2001; Zwally et al., 2005; Rignot et al., 2008; Pritchard et al., 2009; Wingham et al., 2009).

2. Methodology

2.1. Sample collection

A Seabird Scientific SBE911plus conductivity-temperature-depth (CTD) instrument with a 24 bottle rosette was used to vertically profile the water column and collect water for organic geochemical analysis. Water was collected on board the *RRS* James Clark Ross (expeditions JR272 and JR257) during March-April 2012 (austral autumn) from 15 stations along the former WOCE A23 section (Meredith et al., 2001) traversing the Scotia Sea between the northern Weddell Sea and South Georgia (Table 1 and Figure 1; Allen et al., 2012; Venables et al., 2012), and on board the *R/V* Polarstern expedition PS104 during February-March 2017 (austral summer) from 5 stations in the Amundsen Sea embayment (Table 2 and Figure 1; Gohl, 2017). Water samples were collected in 10 L Niskin bottles. In the Scotia Sea, the depth of the sample collection was dependent on the expression of the mixed layer and seasonal thermocline as observed during each CTD deployment. At all stations, a "mixed layer" sample was collected between 10-40m depth and a "thermocline layer" sample collected between approximately 60-110 m depth (Table 1). In the Amundsen Sea, the sampling strategy included samples from surface thermocline waters, and CDW. Water samples (approximately 10-30 L) were vacuum filtered through pre-combusted GF/F filters (Whatman, 0.7 µm pore size, 50 mm diameter). Glass fibre filters with a nominal pore size of 0.7 µm are most commonly used for sampling of SPM in ocean and lake waters. However, as microbes can range in size from 0.2-0.7 µm, these filters may lead to an under-sampling of archaeal cells that are not associated with aggregates (Lee et al., 1995; Ingalls et al., 2012). Therefore, IPL-GDGT concentrations reported here represent the minimum likely concentrations.

The filters were subsequently stored in foil at -20 °C, then transported to Durham University (UK; Scotia sea samples) and Alfred Wegener Institute (Germany; Amundsen Sea samples). Samples were freeze-dried prior to lipid extraction.

https://doi.org/10.5194/bg-2020-333
Preprint. Discussion started: 5 November 2020


Biogeosciences Discussions

2.2. Sample extraction

Total lipids of the Scotia Sea sample set were extracted at the Royal Netherlands Institute for Sea Research. Freeze-dried samples were extracted using a modified Bligh and Dyer methodology as detailed in Besseling et al. (2018). Briefly, sample filters were cut into small pieces using solvent cleaned scissors. The total lipids were extracted using a monophasic mixture of K_2HPO_4 (8 g/L adjusted to pH 7-8), dichloromethane (CH_2Cl_2) and methanol (CH_3OH) at a ratio of 0.8:1:2. Extractions were repeated three times and pooled. The pooled extract was subsequently phase separated by adjusting the ratio of K_2HPO_4: CH_2Cl_2: CH_3OH to 0.9:1:1. The CH_2Cl_2 layer of the resultant bi-phasic mixture was transferred to a round bottom flask. This was repeated three times, with the Bligh Dyer extract (BDE) dried under a stream of N_2.

Total lipids of the Amundsen Sea sample set were extracted at the Alfred Wegener Institute (Germany). Freeze dried samples were extracted ultrasonically using CH_2Cl_2 and CH_3OH at a ratio of 2:1 for 15 minutes. This was repeated three times, the extracts pooled and dried under a stream of N_2. The resulting total lipid extract was fractionated over a silica column using hexane (for elution of the alkanes and highly branched isoprenoids) followed by CH_2Cl_2:hexane and CH_2Cl_2:CH_3OH both at a ratio of 1:1 for elution of the polar fraction. The polar fraction was dried under N_2 and stored at -20 °C prior to IPL analysis. The method used for the extraction of the Amundsen Sea samples is not the regular IPL extraction procedure as it, for example, does not use phosphate buffer and that this may have an influence of the results obtained for the Amundsen Sea samples.

An internal standard of 1-O-hexadecyl-2-acetyl-*sn*-glycero-3-phosphocholine was added to both the Amundsen and Scotia Sea samples. The TLE (Scotia Sea) and polar fraction (Amundsen Sea) were filtered through true regenerated cellulose filters (4 mm, 0.45 µm pore size) using hexane, propan-2-ol, and water at a ratio of 79:20:1. Samples were stored at -20 °C prior to analysis.

2.3. Intact Polar Lipid characterisation

IPL-GDGTs were analysed using a modification of the Sturt et al. (2004) methodology as detailed in Besseling et al. (2018). To summarise, an Agilent 1290 Infinity I UHPLC, equipped with a thermostated auto-injector and column oven, coupled to a Q Exactive Orbitrap MS with Ion Max source with a heated electrospray ionisation (HESI) probe (Thermo Fisher Scientific, Waltham, MA, USA). Separation was achieved using a YMC-Triart Diol-HILIC column (250 x 2.0 mm, 1.9 µm particle size, 12 nm pore size;

https://doi.org/10.5194/bg-2020-333
Preprint. Discussion started: 5 November 2020

YMC co., Ltd., Kyoto, Japan) maintained at 30 °C with a flow rate of 0.2 mL/min. Chromatographic separation of IPL-GDGTs was achieved using the following 70 minute program: 0% eluent B from 0-5 minutes, linear gradient to 34% eluent B at 25 minutes, isocratic 25-40 minutes, linear gradient to 60% B at 55 minutes, linear gradient to 70% B 65 minutes, followed by a re-equilibration time of 20 minutes between each analysis. Eluent A was hexane/propan-2-ol/formic acid/ 14.8 M NH_{3aq} (79:20:0.12:0.04 [v/v/v/v]), eluent B is propan-2-ol/water/formic acid/14.8 M NH_{3aq} (88:10:0.12:0.04 [v/v/v/v]). HESI sheath gas, auxiliary gas and sweep gas N_2 pressures were 35, 10, and 10 (arbitrary units) respectively with the auxiliary gas at 50 °C. The spray voltage was 4.0 kV (positive ion ESI), S-Lens 70 V, and capillary temperature 275 °C. Mass range monitored was between *m/z* 375 and 2000 (resolving power of 70 000 ppm at *m/z* 200) followed by data dependent fragmentation of the 10 most abundant masses in the mass spectrum (with the exclusion of isotope peaks) were fragmented successively (stepped normalised collision energy 15, 22.5, 30; isolation window 1.0 m/z). A dynamic exclusion window of 6 s was used as well as an inclusion list with a mass tolerance of 3 ppm to target specific compounds (absolute *m/z* values of IPL-GDGTs can be found in supplement A). The Q Exactive Orbitrap MS was calibrated within a mass accuracy range of 1 ppm using the Thermo Scientific Pierce LTQ Velos ESI Positive Ion Calibration Solution (containing a mixture of caffeine, MRFA, Ultramark 1621, and N-butylamine in an acetonitrile-methanol-acetic acid solution). Peak areas for each individual IPL were determined by integrating the combined mass chromatograms (within 3 ppm) of the monoisotopic and first isotope peak of all the relevant adducts formed (protonated, ammoniated, and/or sodiated). IPL-GDGTs were examined in terms of their MS peak area response. Thus, the relative abundance of the peak area does not necessarily reflect the actual relative abundance of the different IPL-GDGTs, however, this method allows for the comparison between samples analysed in this study. The peak areas were determined from extracted ion chromatograms of the $[M+H]^+$, $[M+NH_4]^+$, and $[M+Na]^+$ for each individual IPL-GDGT species. C-GDGT lipids were not analysed.

2.4. Data Analysis

Standards for individual IPL-GDGTs are not available therefore; concentrations reported here are semi-quantitative. IPL-GDGT peak areas were normalised to the internal standard and volume of water filtered and are reported as units/L. The Ring Index (RI) was calculated based on Zhang et al. (2016).

https://doi.org/10.5194/bg-2020-333
Preprint. Discussion started: 5 November 2020

225 Redundancy analysis (RDA) was performed on the Scotia Sea data set in RStudio (version 1.2.1335) using
226 Vegan and Faraway packages. RDA was performed using data normalised to the internal standard and total
227 water volume extracted (scaled). Temperature, salinity, oxygen concentration, and Chlorophyll A
228 fluorescence (hereafter referred to as fluorescence) were selected as explanatory variables and IPL-GDGT
229 relative abundances are the response variables. Statistical significance of RDA, axes, and explanatory
230 variables were determined using an Anova-like test (Legendre et al., 2011).

231 **3. Results**

232 **3.1. Physicochemical properties of the water column**

233 CTD measurements were taken at all 5 stations in the Amundsen Sea; PS104/003, PS104/007, PS104/017,
234 PS104/022, PS104/043. Temperature – salinity (T-S) plots are shown in Figure 2. Temperature, salinity,
235 fluorescence, oxygen profiles are shown for each of the Amundsen Sea stations in Supplement B S1. At the
236 time of sampling, water masses in the Amundsen Sea study area were characterised by a temperature range
237 of -1.7 to +1.1 °C, a salinity range of 32.8 to 34.7 PSU, and an oxygen concentration of between 4.5 and 8.9
238 ml/L (Supplement B S1). Ocean temperatures in the Amundsen Sea, generally show a relatively warm
239 surface layer, followed by a steep thermocline to a temperature minimum (winter water) extending down to
240 approximately 400m, with ocean temperatures increasing below this point due to the intrusion of relatively
241 warm CDW (Supplement B S1). Three different water masses are detected in the Amundsen Sea from the T-
242 S plot: AASW, CDW, and modified CDW (Figure 2). Fluorescence peaked at the surface within the
243 uppermost 20 m, followed by a steep decline with depth (Supplement B S1). High fluorescence values were
244 observed at PS104/017 with 8mg/m^3, and PS104/007 with 4 mg/m^3 respectively, whereas low fluorescence
245 values were observed at stations PS104/003, PS104/022, and PS104/043 (Supplement B S1).
246 The Scotia Sea study area encompasses the SAF, PF, SACCF and the SBACC (Figure 1a) and is
247 characterised by a temperature range of -1.6 to +7.3 °C, and a salinity range of 33.6-34.7 PSU (Figure 2).
248 The temperature range of the mixed layer samples was -1.2 to +7.3 °C and thermocline samples was -1.6 to
249 +6.1 °C. A clear partition between the sample stations is observed in the T-S plot (Figure 2) with consistently
250 higher water temperatures found at stations north of CTD 19 and on average lower ocean temperatures south
251 of CTD 18. This region broadly marks the location of the SBACC at ~58.6 °S (Figure 1a).

https://doi.org/10.5194/bg-2020-333
Preprint. Discussion started: 5 November 2020

3.2. Intact Polar GDGT inventory

A total of 12 IPL-GDGTs (see Supplement B S2 for structures) were identified within 48 samples from the Southern Ocean (Figure 3 and 4, Tables 3 and 4). This included IPLs with cores comprising of GDGT-0, GDGT-1, GDGT-2, cren, OH-GDGTs-0, and diOH-GDGT-0. It should be noted that the LC-MS method utilised in this study does not separate individual GDGT isomers, including crenarchaeol (cren) and its isomer, cren', and hence the cren detected here is likely a combination of both isomers. The majority of the IPL-GDGTs in both the Amundsen and Scotia seas were regular GDGTs (i.e. not hydroxylated) with a mean contribution of 69% (±20%) and 66% (±18%) respectively (excluding samples where IPL-GDGTs were absent). diOHGDGT-0 was the least common core lipid identified in the Scotia and Amundsen Sea. Both forms of hydroxyl-GDGT were observed with zero cyclopentane moieties (OH-GDGT-0 and diOH- GDGT-0). While GDGT-1, GDGT-2, and cren were detected, GDGT-0 was the dominant regular GDGT in both the Amundsen and Scotia seas. GDGT-0, cren, and OH-GDGT-0 were all detected in combination with the MH, DH, and HPH head groups. GDGT-1 and GDGT-2 were only found to be associated with DH and diOH-GDGT-0 was only found in combination with MH (Tables 2 and 3).

3.3. Amundsen Sea depth profiles

Archaeal IPLs were identified in the water column at all Amundsen Sea stations. The relative abundance of the regular GDGT core (i.e. non-hydroxylated) varied with depth ranging from 20-100% of total IPL-GDGTs (excluding depths where no IPL-GDGTs were identified; Table 4). PS104/003 and PS104/007 were found to have IPL-GDGTs in the uppermost surface sample (10 m and 20 m depths respectively). The surface sample at PS104/003 (10m) was dominated by non-hydroxylated GDGTs (94.3% of total IPLs) with a lower relative abundance of OH-GDGT core type (5.7% of total IPLs). Further to this, HPH-GDGT-0 was the most abundant IPL-GDGT at this station (81.8% of total IPLs) with HPH-cren contributing a smaller fraction of the total IPL-GDGTs (11.1%). Low relative abundance of MH-GDGT-0 (<1%), MH-cren (<1%), MH-OH-GDGT-0 (<1%), DH-OH-GDGT-0 (5.1%), and MH-diOH-GDGT-0 (<1%) were also observed at PS104/003 10 m. This contrasts with the surface sample at PS104/007 (20 m) where no OH-GDGT-IPLs were detected and where the IPL-GDGT suite is split between MH-GDGT-0 (89.1%) and MH-cren (10.9%). IPL-GDGTs were not identified within the surface sample at PS104/017 (10 m) and the two mid-shelf stations, PS104/022 (10 m and 30 m) and PS104/043 (10 m). DH-GDGT-0 and DH-cren are minor

https://doi.org/10.5194/bg-2020-333
Preprint. Discussion started: 5 November 2020

components of the IPL-GDGT suite with maximum relative abundance observed in the deepest samples for all Amundsen Sea stations. The relative abundance of IPL-GDGTs with a MH head group peaks in the mid depths between 120 and 240 m (with the exception of the surface 20 m at PS104/007). Further to this, the ratio of MH/DH and MH/HPH is also highest at the mid depths between 120 and 240 m (Table 5 and 6). The ratio of GDGT-0/cren is variable throughout the Amundsen Sea stations, ranging from 2.8-8.2 (excluding samples with no GDGTs). The sample taken from 180 m water depth at PS104/003 exceeded this range with a GDGT-0/cren ratio of 27.0 (Table 5 and 6).

3.4. Scotia Sea transect

Archaeal IPLs were detected within all 16 Scotia Sea stations. A clear depth trend in IPL-GDGTs can be observed where IPL-GDGTs were detected in the thermocline samples but were often below detection within the mixed layer. Exceptions to this are CTD 1, 16, 20, and 21 where IPL-GDGTs were present in both the mixed and thermocline layers. Relative abundance (%) of IPL-GDGT cores and the degree of cyclicity remains constant along the Scotia Sea transect with IPL-GDGT head groups showing greater variation along the transect. An increase in the relative abundance of the HPH head group is observed within the thermocline samples between CTD 22 (53.5 °S) and 5 (63.3 °S) this is coupled with a decrease in the relative abundance (%) of MH and DH IPL-GDGT head groups (Figure 3b). Mixed layer CTD 20 and 21 are dominated by MH, CTD 16 is dominated by HPH, and CTD 1 mixed layer contains a mixture of all three IPL-GDGT head groups. The GDGT-0/cren ratio generally ranges from 1.6-9.9, but CTD 7 (21.7), 10 (177.6), and 16 (16.8), located at the thermocline, exceed this range due to low cren concentrations (Table 5). In preparation for RDA, biomarkers that were identified in fewer than three samples were designated “rare species” and were excluded from the analysis (GDGT-DH-0, GDGT-DH-1 and OH-GDGT-HPH-0 excluded). This is because outliers can violate the linearity of the relationship between the response and explanatory variables (Legendre & Legendre, 2012). Samples 1 and 25 were also excluded from the analysis. Sample 1 is located offshore of the Falkland Islands and is the only sample from North of the SAF, thus representing the only data point for the Subantarctic Zone of the Southern Ocean that is unlikely to be representative for the polar environment. Sample 25, located close to South Georgia, was excluded due to high biomarker abundances (Figure 3a) which could be due to exceptionally high productivity in this area (e.g. Atkinson et al., 2001). Variance inflation factors (VIFs) for the response variables were between 3.5 (fluorescence) and 11.4

https://doi.org/10.5194/bg-2020-333
Preprint. Discussion started: 5 November 2020

(oxygen concentration) (Supplement C). The VIF for oxygen concentration is slightly higher than is typically acceptable for RDA analysis. This is due to correlation between oxygen concentration and fluorescence (R_2=0.62), however, as the R_2 is below 0.7 this is unlikely to violate the assumptions of the RDA (Legendre & Legendre, 2012). RDA shows 64% constrained variation with RDA1 and 2 accounting for 63% of the cumulative variation. The RDA is statistically significant (p=<0.05, f=3.5), furthermore, RDA1 is found to be statistically significant (p=<0.05, f=11.48) however, RDA2 is not significant (p=0.42, f=2.35). Species scores show HPH-GDGT-0 and HPH-cren to load positive on RDA 1, with MH-GDGT-0, MH-cren, MH-OH-GDGT-MH-0, DH-OH-GDGT-0, and MH-MH-diOH-GDGT-0 loading highly negative on RDA1. Of the explanatory variables tested, temperature is statistically significant at the <0.05 level (f=8.56) and with salinity (p=0.07, f=2.61) and oxygen concentration (p=0.09, f=2.58) approaching significance. The site scores show CTD 20, 21, 22, 23, and 24 to be negatively loaded on RDA1 with CTD 3, 5, 7, 10, 13, 16, 18 and 19 to be positively loaded on RDA1 suggesting that these stations are contrasted along this axis.

4. Discussion

4.1. Hydroxylated GDGTs in Polar Environments

In this study, two hydroxylated GDGTs (OH-GDGT-0 and diOH-GDGT-0) were detected. Hydroxylated GDGTs have been reported as potential biomarkers for reconstructing ocean temperature change in cold waters (Fietz et al., 2013, 2016) and in this study contribute up to 49.8% (OH-GDGT) and 30.1% (diOH-GDGT) of total IPL-GDGTs. Hydroxylated IPL-GDGTs are not commonly reported in previous SPM studies (e.g. Kim et al., 2016; Kang et al., 2017; Hurley et al., 2018). However, these compounds have been reported as c-GDGTs in marine and lacustrine sediments, with hydroxylated GDGTs found to contribute approximately 8% in marine sediments from temperate and tropical sites (Liu et al., 2012; Lu et al., 2015). These compounds have been reported in much higher abundance in polar environments including up to 20% in SPM and up to 16% in surface sediments from the Nordic Seas (Fietz et al., 2013) and up to 20% in surface sediments from the Southern Ocean (Huguet et al., 2013).

In the Amundsen and Scotia seas, hydroxylated GDGTs made up a significant amount of the total IPL-GDGT profile, contributing up to 79.9% (Amundsen Sea, PS104/003 - 180 m). Even excluding this one exceptional sample, hydroxylated IPL-GDGT abundances were still consistently above 20% with a maximum relative abundance of 48.1% in the Amundsen Sea and 68.5% of total IPL-GDGTs in the Scotia

https://doi.org/10.5194/bg-2020-333
Preprint. Discussion started: 5 November 2020

Sea (Table 3 and 4). Exceptionally high hydroxylated GDGT relative abundances could be due to differences in methodologies to the previous studies which measured core GDGTs by atmospheric pressure chemical ionisation (APCI; Liu et al., 2012; Fietz et al., 2013; Huguet et al., 2013; Lu et al., 2015) while this study examined IPL-GDGTs using electrospray ionisation (ESI). Using the same LC-MS methodology, Sollai et al. (2019a) report average hydroxylated IPL-GDGT relative abundances of 22% (±19%) with a range of 0-51% in SPM from the euxinic Black Sea; however, similar analyses from the Arabian Sea (Besseling et al., 2018), the eastern tropical South Pacific (Sollai et al., 2019b) and the Mediterranean Sea did not detect hydroxylated IPL-GDGTs. Molecular dynamics simulations have shown that the addition of hydroxyl moieties in the tetraether structure increases the fluidity of the cell membrane and aid trans-membrane transport in cold environments (Huguet et al., 2017). The exceptionally high amount of hydroxylated IPL-GDGT for the Amundsen and Scotia seas may therefore be due to elevated synthesis of these biomarkers in cold environments.

4.2. IPL-GDGT Distributions as an Indicator of Archaeal Populations

In both the Amundsen and Scotia Sea samples GDGT-0 dominated the IPL-GDGT profiles contributing up to 89.1% of the total in the Amundsen Sea and up to 100% in the Scotia Sea. Low diversity of cyclic GDGTs in this study is indicated by RI ranging from 0.02 – 1 for the Scotia Sea and 0.03 – 0.9 for the Amundsen Sea (Tables 5 and 6). This is particularly low compared with the RI of the global core top calibration, which includes a range of Southern Ocean samples, reporting an RI range of 1.25-3 (excluding the Red Sea samples) (Kim et al., 2010; Ho et al., 2011, 2014; Zhang et al., 2016). Previous SPM studies spanning a range of marine habitats have reported the presence of hydroxylated GDGT-1, -2, and -3 as well as a wider range of non-hydroxylated GDGTs, such as GDGT-3 and -4 (Kim et al., 2016; Besseling et al., 2018; Hurley et al., 2018; Sollai et al., 2019a,b). As this study used the same analytical methodology as Besseling et al. (2018) and Sollai et al. (2019a,b), these differences cannot be attributed to analytical methodologies. Low cyclic diversity of GDGTs in the Amundsen and Scotia seas could be due to differences in the synthesis of these lipids by the source Thaumarchaeota. The relationship between ocean temperature and the cyclicity of GDGTs has been firmly established, with increasing ocean temperatures correlated with increasing relative abundance of GDGTs with 2 or more cyclopentane moieties (Schouten et al., 2002, 2007; Kim et al., 2008, 2010). However, Kim et al. (2010) note some differences between sub-tropical and sub-polar oceans, with

https://doi.org/10.5194/bg-2020-333
Preprint. Discussion started: 5 November 2020

364 cren playing a more important role in temperature reconstructions in the subtropics than in polar oceans,
365 suggesting that there may be differences in membrane adaptation strategies of Thaumarchaeota. Principal
366 component analysis of IPL-GDGT distributions of a moderately thermophilic Thaumarchaeota along with
367 previously published data identifies two distinct clusters with a clear partition between the orders of
368 Nitrosopumilales and Nitrososphaeales (Bale et al., 2019). GDGTs analysed in this study cluster within the
369 Nitrosopumilales group due to the high relative abundances of GDGT-0 and low relative abundances of all
370 other GDGTs. Due to the polar locations of the Amundsen and Scotia Sea samples, Nitrosopumilales are
371 likely to be the key AOA in these environments. Previous microbial analysis of the spatial variation in
372 prokaryotes of the Amundsen Sea polynya identified the most abundant Thaumarchaea marine group I
373 (MGI) sequence belonged to the cluster affiliated with "*Ca. Nitrosopumilus maritimus*" (Kim et al., 2014). In
374 similar studies within the wider Southern Ocean region phylogenetic analysis reveals high abundances of
375 sequences clustering with *Nitrosopumilus*. Hernandez et al. (2015) analysed surface water samples from
376 Potter Cove (King George Island, wester Antarctica Peninsula) which revealed that the majority of sequences
377 fell into the clade containing "Ca. *Nitrosopumilus maritimus"* and other environmental sequences containing
378 Thaumarchaeota. Signori et al. (2018) studied microbial spatial and temporal variability at 10 stations off the
379 Antarctic peninsula revealing spring to be characterised by SAR11 and microbial communities remaining
380 from winter, including Thaumarchaeota (*Nitrosopumilus*), Euryarchaeota, and SAR324, with a shift in
381 microbial populations during the summer and autumn.
382 Three polar head groups were detected in this study, i.e. MH, DH, and HPH. All three head groups have
383 previously been identified in culture (Schouten et al., 2008; Pitcher et al., 2011; Sinninghe Damsté et al.,
384 2012; Elling et al., 2017), environmental studies (e.g. Zhu et al., 2016; Besseling et al., 2018), and have
385 widely been associated with Thaumarchaeota. It has been postulated that specific IPL-GDGTs may be
386 associated with particular Thaumarchaeotal groups or habitats (Sinninghe Damsté et al., 2012; Elling et al.,
387 2017; Bale et al., 2019). Previously the HPH head group has been associated with the Nitrosopumilales order
388 (Group I.1a) and the DH head group with the Nitrosophaeales order (Group I.1b) (Sinninghe Damsté et al.,
389 2012). More recent studies have shown that environmental niche or habitat may be the main driver of GDGT
390 head group composition rather than phylogeny (Elling et al., 2017; Bale et al., 2019). Relevant to this study,
391 Elling et al. (2017) analysed the lipidome of 10 Thaumarcheotal cultures and identified DH-GDGTs and DH-
392 OH-GDGTs as key membrane components of the marine mesophiles compared with the terrestrial

https://doi.org/10.5194/bg-2020-333
Preprint. Discussion started: 5 November 2020

393 thermophilic and soil mesophilic Thaumarchaeota. In the present study, high abundances of HPH were
394 detected, contributing up to 92.9% and up to 100% of total IPL-GDGTs in the Amundsen Sea and Scotia Sea
395 respectively. The dominance of HPH in the lipid profiles of the Amundsen and Scotia seas align with
396 previous culture analysis (Schouten et al., 2008; Pitcher et al., 2011; Sinninghe Damsté et al., 2012; Elling et
397 al., 2017).

398 **4.3. Influence of Circumpolar Deep Water on IPL Distributions: Amundsen Sea**

399 In this study, we observed a number of consistent trends in the water column IPL-GDGT distributions
400 between the different Amundsen Sea sampling stations. In the surface samples, collected within the euphotic
401 zone at PS104/017 (10 m), PS104/022 (10 m and 30 m), PS104/043(10 m), no IPL-GDGTs were identified.
402 Previous studies from the Southern Ocean have shown water column archaeal distributions to be highly
403 variable on both a temporal and spatial scale. Broadly, archaea (as measured by cell counts or rRNA) are
404 often absent or found in relatively low abundance in the surface waters during the austral spring algal bloom
405 and during austral summer (Massana et al., 1998; Church et al., 2003; Kalanetra et al., 2009; Besseling et al.,
406 2020). The absence of archaea in the surface waters of the Southern Ocean contrasts with the high abundance
407 of bacteria and is part of a larger seasonal cycle in archaeal population dynamics (Church et al., 2003).
408 Temporal distributions of archaea are then shown to become more evenly distributed by depth, with an
409 increase in the population within the surface waters throughout austral autumn-winter (Church et al., 2003).
410 The Amundsen Sea samples were collected during austral summer. Two previous studies in the Antarctic
411 Peninsula show an increase in group I archaeal populations in surface waters during austral summer and
412 winter (Massana et al., 1998; Murray et al., 1998). However, Kalanetra et al. (2009) did not observe any
413 archaea in surface waters west of the Antarctic Peninsula during austral summer. The mechanism for this
414 temporal heterogeneity is likely mediated by a combination of physical and biological factors including,
415 water mass properties, concentrations of dissolved and particulate organic carbon (Murray et al., 1998).
416 Furthermore, the absence of AOA in the surface waters during austral spring, when primary productivity is
417 highest, could be due to competition with bacteria and algae that bloom during the same time period and/or a
418 subsequent nutrient limitation (Massana et al., 1998; Church et al., 2003; Kalanetra et al., 2009). As the
419 current study was only performed at one time point during austral summer a larger sampling campaign
420 would be required to fully characterise microbial and IPL-GDGT seasonality in the Amundsen Sea.

https://doi.org/10.5194/bg-2020-333
Preprint. Discussion started: 5 November 2020

In contrast to the other stations, the surface water samples from PS104/003 and PS104/007 (10 m and 20 m respectively) were found to contain IPLs. Unusually, the samples from PS104/007 (10 m) only contained the MH head group. It should be noted that while the MH head group is known to be synthesised by archaea (e.g. Sinninghe Damsté et al., 2012), this IPL is recalcitrant and can be formed as a degradation product of other IPL-GDGTs (e.g. Lengger et al., 2013, 2014). In contrast, HPH is more labile and less readily preserved in sediments following cell death and is hence considered to be a biomarker for recently active archaea and, in particular, Thaumarchaeota (Pitcher et al., 2010; Sinninghe Damsté et al., 2012). While DH head group is not as labile as HPH due to its glycosidic structure (Lengger et al., 2013), the prevalence of DH across the Thaumarchaeota phylum may suggest some use of this head group as a biomarker for the archaeal community (Elling et al., 2017). Hence, the dominance of the MH head group at this station may indicate an inactive/relic archaeal population at this depth. Higher IPL-GDGT diversity was detected at PS104/003 including HPH and DH head groups indicating a recently active archaeal population (Sinninghe Damsté et al., 2012; Elling et al., 2017). PS104/003 is located in an area of active upwelling of nutrient-rich waters largely composed of CDW (Pine Island Bay polynya) (Mankoff et al., 2012). Together with the Amundsen Polynya located north of Dotson and westernmost Getz ice shelves (Figure 1), it is one of the most productive regions (per unit area) of the Southern Ocean (Arrigo and van Dijken, 2003). Productivity is further aided by the influx of iron released from the rapidly melting Thwaites and Pine Island glaciers (Alderkamp et al., 2012; Gerringa et al., 2012; Thuroczy et al., 2012; St-Laurent et al., 2017). Productivity in this area is not only limited by nutrient and iron availability but also by light; productivity is 30-50% lower in the Pine Island Polynya compared to the Amundsen Polynya, with this difference attributed to the significant difference in solar irradiance levels between the two polynyas throughout the summer season (Park et al., 2017). Kalanetra et al. (2009) suggests that a combination of both light and nutrient differences between Arctic and Antarctic ocean settings could cause the differences in archaeal populations in the surface ocean, where low light and nutrient levels in the surface allows archaeal populations to flourish, with further studies suggesting photoinhibition of Thaumarchaeota (Church et al., 2003; Mincer et al., 2007; Hu et al., 2011; Merbt et al., 2012; Luo et al., 2014).

IPL-GDGT diversity increased downwards in the water column through the thermocline and the CDW layer in the Amundsen Sea (Figure 4). DH-cren and HPH-cren may be widely applied as biomarkers for recently active Thaumarchaeota populations having been identified as key cell membrane lipids (Pitcher et al., 2010;

https://doi.org/10.5194/bg-2020-333
Preprint. Discussion started: 5 November 2020

Sinninghe Damsté et al., 2012; Elling et al., 2017). HPH-cren was identified consistently throughout the thermocline and CDW layer at all Amundsen Sea stations (Table 4). Our results, therefore, suggest recently active AOA at the thermocline and within the CDW. Tolar et al. (2016) shows ammonia oxidation (AO) to occur throughout the water column, with similar rates of AO in CDW during both winter and summer seasons and increased AO in surface waters during the late winter in sites west of the Antarctic Peninsula. This is consistent with molecular microbiology studies from the Amundsen Sea and Antarctic Peninsula region that identify Thaumarchaeota throughout the water column, but with a seasonal trend where these archaea are often absent in the surface waters during spring and summer, and present in the CDW throughout the season (Massana et al., 1998; Alonso-Saez et al., 2011). HPH-cren, however, may not be the most suitable proxy for tracking the complete AOA population as the relative abundance of this IPL can vary significantly between phylogenetic subgroups (Elling et al., 2017). DH-GDGTs have been identified with consistent relative abundances across the Nitrosopumilales order (Group 1.1a), suggesting DH-cren as an additional biomarker for AOA activity (Elling et al., 2017). In this study we detect DH-cren consistently in the CDW layer and with low relative abundance in the thermocline of PS104/003 and PS104/007 and absence in the thermocline waters at PS104/017 and PS104/022. Thaumarchaeota are thought to partition between shallow water (0-130 m) and deep water (500-4000 m) marine clades (Francis et al., 2005; Hallam et al., 2006). Therefore, this difference in HPH-cren and DH-cren distributions could reflect differences in Thaumarchaeota populations in the Amundsen Sea. While the data presented here provide only a snapshot of the Amundsen Sea IPL-GDGT distributions, this small contrast in HPH and DH-cren distributions may represent a significant partition between Thaumarchaeota populations and warrants further analysis.

4.4. Influences on the GDGT-IPL distribution along the Scotia Sea Transect

Samples from the Scotia Sea were taken along a transect spanning 54 °S – 64 °S (Figure 1a). The T-S plot (Figure 2) shows the CTD profiles for stations taken along the transect between 64 °S and 58.6 °S (CTD 3-21) located south of the SBACC and stations between 53 °S and 58.6 °S (CTD 1, 22-25) located in the Antarctic zone between the SBACC and the PF (Figure 1a). Results show IPL-GDGTs to be absent from the mixed layer samples (15-40 m). Samples were collected between March and April 2012 and, similar to the Amundsen Sea, the absence of IPL-GDGTs at these stations could be due to photo-inhibition and competition from bacteria and algae at the surface (Church et al., 2003; Mincer et al., 2007; Hu et al., 2011;

https://doi.org/10.5194/bg-2020-333
Preprint. Discussion started: 5 November 2020

Merbt et al., 2012; Luo et al., 2014). IPL-GDGTs are present at the surface CTD 1, 21, 20, and 16. CTD 21 and 20 are dominated by MH, which implies relic and not active archaeal populations (Lengger et al., 2013, 2014). CTD 16 contains low relative abundances of HPH-GDGT-0 which could indicate some archaeal activity. However, CTD 1 contains greater IPL diversity including DH and HPH head groups potentially suggesting a recently active archaeal community at the surface. CTD 1 is located close to the Falkland Islands in the Subantarctic Zone north of the SAF and is potentially subject to additional terrestrial inputs and coastal dynamics.

IPL-GDGTs were also found to be present within the thermocline (60-110 m) and contain a high proportion of MH head group IPLs, suggesting a high proportion of relic IPL-GDGTs in the Scotia Sea that could relate to variability in seasonality of archaeal populations. Further to this, DH-cren was found to be absent from the thermocline, with HPH-cren intermittently present. This is consistent with our results from the Amundsen Sea where DH-cren was mostly absent from the 120-240m depth intervals but present in the CDW depth intervals (i.e. below 400m), while HPH-cren was present at both the thermocline and CDW depths.

As noted above, the Scotia Sea samples were collected along clear temperature (-1.6 to +7.3 °C), salinity (33.6 -34.3 PSU), oxygen (218.3-332.7 ml L^{-1}), and fluorescence (0.03-1.1 ml m^{-3}) gradients associated with ocean fronts, which are known to impact bacterioplankton population diversity (Wilkins et al., 2013; Baltar et al., 2016; Raes et al., 2018). Figure 5 shows that higher latitude samples with cooler ocean temperatures cluster positively on RDA axis 1 and have higher relative abundances of HPH-GDGT-0 and HPH-cren (samples 3, 5, 7, 10, 13, 16, 18, 19), whilst samples from warmer ocean waters and lower latitudes cluster negatively on RDA axis 1 and have higher relative abundances of MH and DH IPL-GDGTs (samples 20 – 24). This suggests that RDA 1 represents the transition across the SBACC. Temperature was found to be statistically significant explanatory variable in the RDA which is consistent with previous research that has identified clear links between core GDGT relative abundances and environmental variables such as temperature (Schouten et al., 2007; Kim et al., 2008, 2010). Specifically, we observe a shift in the GDGT head group between the warmer and cooler waters of the ACC fronts. Temperature, along with other physicochemical properties (e.g. nutrient and oxygen concentrations) vary across the ACC (e.g. Rubin, 2003; Freeman et al., 2019). These shifts in physicochemical properties across permanent oceanic boundaries influence and control bacterial and archaeal species richness, creating ecological boundaries or niches (e.g. Raes et al., 2018). Variability in IPL-GDGT headgroup composition observed across the Scotia Sea transect

https://doi.org/10.5194/bg-2020-333
Preprint. Discussion started: 5 November 2020

could reflect the transition across an environmental niche (e.g. Elling et al., 2017; Bale et al., 2019). As this study is limited by the number of chemical properties analysed, it would be speculative to infer the relative importance of specific nutrient concentrations across the Scotia Sea transect.

Alternatively, the shift in IPL-GDGT head group could also be influenced by the presence of the Weddell Gyre which is located south of 55-60 °S, and between 60 °W and 30 °E (Deacon et al., 1979). The Weddell Gyre is a region of enhanced productivity, with austral summer chlorophyll A concentrations ranging from 1.5-10 µg/L (Bathmann et al., 1997; Cape et al. 2014) due to high concentrations of nutrients upwelled and circulated through the gyre (Vernet et al., 2019 and references therein).

5. Conclusions

A range of archaeal IPLs were detected in both the Amundsen Sea and the Scotia Sea. High relative abundances of OH-GDGT core type were observed which could reflect the polar environmental setting of these samples. Low cyclicity was detected for both the GDGT and OH-GDGT core type with acyclic OH-GDGT-0 and GDGT-0, -1, -2, and cren reported.

In the Amundsen Sea a high relative abundance of IPL-GDGTs throughout the water column is indicative of Thaumarchaeota activity both within the thermocline and CDW. Indeed, the Thaumarchaeotal populations within CDW could make a significant GDGT contribution to the sedimentary record which could have implications for GDGT based temperature reconstructions.

IPL-GDGT relative abundance along the Scotia Sea transect shows a distinct pattern across the oceanographic front transition. Samples south of the SBACC and from cooler ocean waters having higher relative abundances of HPH-GDGT-0 and HPH-cren compared with samples north of the SBACC, and from warmer ocean waters having higher relative abundances of MH and DH IPL-GDGTs. Indeed RDA reveals that temperature is a significant explanatory variable, however, productivity and nutrient availability may also play a role in IPL-GDGT distributions. Additionally, this shift in IPL-GDGT distributions could represent a shift in the dominant archaeal IPL synthesisers and/or a physiological survival strategy.

Data availability

CTD data from JR257/JR272A are available from the British Oceanographic Data Centre at https://www.bodc.ac.uk/data/documents/cruise/11431/.

https://doi.org/10.5194/bg-2020-333
Preprint. Discussion started: 5 November 2020

535 Author contributions

536 CSJ, ELM, CDH, EM, JAS designed the experiments. CSJ, NJB, ECH, JM undertook the laboratory
537 preparation and analysis. PV, CA, TB, VP generated the oceanographic data. CSJ and AS undertook
538 statistical analysis. CSJ, ELM, NJB, ECH, SS, JAS wrote the manuscript with contributions from all authors.

539 Competing interests

540 The authors declare that they have no conflicting interests.

541 Acknowledgments

542 This project was funded through a UK Natural Environment Research Council (NERC) Standard Grant,
543 awarded to JS, ELM, CDH, and Kate Hendry (NE/M013081/1), a British Antarctic Survey Collaborative
544 Gearing Scheme award (ELM), a Helmholtz Research Grant (VH-NG-1101; JM), and the Durham
545 University Department of Geography Research Development Fund (CSJ). N.B. is funded by the European
546 Research Council (ERC) under the European Union's Horizon 2020 research and innovation program (grant
547 agreement no.694569). Collection of CTD casts on the A23 transect was supported by NERC National
548 Capability funding to BAS. We thank M.D. West, A.J. Hayton, and D. Dorhout for technical support. We
549 are grateful to the captains, crews, support staff and scientists participating in cruises JR257, JR272 and
550 PS104, and acknowledge funding for cruise PS104 by AWI, MARUM, BAS and NERC UK-IODP.

551 **6. References**

552 Alderkamp, A.-C., Mills, M. M., van Dijken, G. L., Laan, P., Thuroczy, C.-E., Gerringa, L. J. A., de Baar, H.
553 J. W., Payne, C. D., Visser, R. J. W., Buma, A. G. J. and Arrigo, K. R.: Iron from melting glaciers fuels
554 phytoplankton blooms in the Amundsen Sea (Southern Ocean): Phytoplankton characteristics and
555 productivity, Deep-Sea Res. Part II- Top. Stud. Oceanogr., 71–76, 32–48,
556 https://doi.org/10.1016/j.dsr2.2012.03.005, 2012.

557 Allen, C. S., Peck, V. L., Graham, A. G. C., Blagbrough, H., Robinson, M. W. and McClymont, E.: RRS
558 James Clark Ross Marine Science Cruises JR257 and JR254e, March-April 2012, British Antarctic Survey,
559 Cambridge, UK, https://www.bodc.ac.uk/resources/inventories/cruise_inventory/reports/jr257_254e.pdf,
560 2012.

561 Alonso-Saez, L., Sanchez, O., Gasol, J. M., Balague, V. and Pedros-Alio, C.: Winter-to-summer changes in
562 the composition and single-cell activity of near-surface Arctic prokaryotes, Environ. Microbiol., 10, 2444–
563 2454, https://doi.org/10.1111/j.1462-2920.2008.01674.x, 2008.

564 Alonso-Saez, L., Andersson, A., Heinrich, F. and Bertilsson, S.: High archaeal diversity in Antarctic
565 circumpolar deep waters, Environ. Microbiol. Rep., 3, 689–697, https://doi.org/10.1111/j.1758-
566 2229.2011.00282.x, 2011.

567 Arrigo, K. and van Dijken, G.: Phytoplankton dynamics within 37 Antarctic coastal polynya systems, J.
568 Geophys. Res. – Oceans., 108, https://doi.org/10.1029/2002JC001739, 2003.

569 Atkinson, A., Whitehouse, M.J., Priddle, J., Cripps, G.C., Ward, P. and Brandon, M.A.: South Georgia,
570 Antarctic: a productive, cold water, pelagic ecosystem, Mar.Ecol.Prog.Ser., 216, 279-308,
571 https://doi.org/10.3354/meps216279, 2001.

572 Bale, N.J., Palatinszky, M., Rijpstra, W.I.C., Herbold, C.W., Wagner, M., Sinninghe Damsté, J.S.:
573 Membrane lipid composition of the moderately thermophilic ammonia-oxidising archaeon "*Candidatus*
574 *Nitrosotenuis uzonensis"* at different growth temperatures. Appl. Environ. Microbiol.,85, https://doi.org/
575 10.1128/AEM.01332-19, 2019.

576 Baltar, F., Currie, K., Stuck, E., Roosa, S. and Morales, S. E.: Oceanic fronts: transition zones for
577 bacterioplankton community composition, Environ. Microbiol. Rep., 8, 132–138,
578 https://doi.org/10.1111/1758-2229.12362, 2016.

579 Bathmann, U.V., Scharek, R., Klaas, C., Dubischar, C.D. and Smetacek, V.: Spring development of
580 phytoplankton biomass and composition in major water masses of the Atlantic sector of the Southern Ocean,
581 Deep Sea Res. Part II Top. Stud. Oceanogr. 44, 51-67, https://doi.org/10.1016/S0967-0645(96)00063-X,
582 1997.

583 Bauersachs, T., Speelman, E. N., Hopmans, E. C., Reichart, G. J., Schouten, S. and Sinninghe Damsté, J. S.:
584 Fossilized glycolipids reveal past oceanic N-2 fixation by heterocystous cyanobacteria, Proc. Natl. Acad. Sci.
585 U. S. A., 107, 19190–19194, https://doi.org/10.1073/pnas.1007526107, 2010.

586 Besseling, M. A., Hopmans, E. C., Boschman, R. C., Sinninghe Damsté, J. S. and Villanueva, L.: Benthic
587 archaea as potential sources of tetraether membrane lipids in sediments across an oxygen minimum zone,
588 Biogeosciences, 15, 4047–4064, https://doi.org/10.5194/bg-15-4047-2018, 2018.

589 Besseling, M. A., Hopmans, E. C., Bale, N. J., Schouten, S., Sinninghe Damsté, J. S. and Villanueva, L.: The
590 absence of intact polar lipid-derived GDGTs in marine waters dominated by Marine Group II: Implications
591 for lipid biosynthesis in Archaea. Sci. Rep., 10, https://doi.org/ 10.1038/s41598-019-57035-0, 2020.

592 Brochier-Armanet, C., Boussau, B., Gribaldo, S. and Forterre, P.: Mesophilic crenarchaeota: proposal for a
593 third archaeal phylum, the Thaumarchaeota, Nat. Rev. Microbiol., 6, 245–252,
594 https://doi.org/10.1038/nrmicro1852, 2008.

595 Cape, M.R., Vernet, M., Kahru, M. and Spreen, G.: Polynya dynamics drive primary production in the
596 Larsen A and B embayments following ice shelf collapse, J. Geophys. Res. Oceans, 119, 572-594,
597 https://doi.org/10.1002/2013JC009441, 2014.

598 Carter, L., McCave, I. N. and Williams, M. J. M.: Circulation and water masses of the Southern Ocean: A
599 Review, Antarct. Clim. Evol., 8, 85–114, https://doi.org/10.1016/S1571-9197(08)00004-9, 2009.

600 Church, M. J., DeLong, E. F., Ducklow, H. W., Karner, M. B., Preston, C. M. and Karl, D. M.: Abundance
601 and distribution of planktonic Archaea and Bacteria in the waters west of the Antarctic Peninsula, Limnol.
602 Oceanogr., 48, 1893–1902, https://doi.org/10.4319/lo.2003.48.5.1893, 2003.

603 Darfeuil, S., Menot, G., Giraud, X., Rostek, F., Tachikaea, K., Garcia, M. and Bard, E.: Sea surface
604 temperature reconstructions over the last 70 kyr off Portugal: Biomarker data and regional modelling,
605 Paleoceanogr. Paleoclimatol. 31, 40-65, https://doi.org/ 10.1002/2015PA002831, 2016.

606 Deacon, G. E. R.: The Weddell gyre, Deep Sea Res. Part I Oceanogr. Res, Pap., 26, 981-995,
607 https://doi.org/10.1016/0198-0149(79)90044-X, 1979.

608 Delong, E. F., Wu, K. Y., Prezelin, B. B. and Jovine, R. V. M.: High abundance of archaea in Antarctic
609 marine picoplankton, Nature, 371, 695–697, https://doi.org/10.1038/371695a0, 1994.

610 Elling, F. J., Konneke, M., Lipp, J. S., Becker, K. W., Gagen, E. J. and Hinrichs, K. U.: Effects of growth
611 phase on the membrane lipid composition of the thaumarchaeon Nitrosopumilus maritimus and their

612 implications for archaeal lipid distributions in the marine environment, Geochim. Cosmochim. Acta, 141,
613 579–597, https://doi.org/10.1016/j.gca.2014.07.005, 2014.

614 Elling, F. J., Konneke, M., Nicol, G. W., Stieglmeier, M., Bayer, B., Spieck, E., de la Torre, J. R., Becker, K.
615 W., Thomm, M., Prosser, J. I., Herndl, G. J., Schleper, C. and Hinrichs, K. U.: Chemotaxonomic
616 characterisation of the Thaumarchaeal lipidome, Environ. Microbiol., 19, 2681–2700,
617 https://doi.org/10.1111/1462-2920.13759, 2017.

618 Etourneau, J., Collins, L. G., Willmott, V., Kim, J. H., Barbara, L., Leventer, A., Schouten, S., Sinninghe
619 Damsté, J. S., Bianchini, A., Klein, V., Crosta, X. and Massé, G.: Holocene climate variations in the western
620 Antarctic Peninsula: evidence for sea ice extent predominantly controlled by changes in insolation and
621 ENSO variability, Clim. Past, 9, 1431–1446, https://doi.org/10.5194/cp-9-1431-2013, 2013.

622 Etourneau, J., Sgubin, G., Crosta, X., Swingedouw, D., Willmott, V., Barbara, L., Houssais, M-N., Schouten,
623 S., Sinninghe Damsté, J.S., Goosse, H., Escutia, C., Crespin, J., Massé, G. and Kim, J-H.: Ocean temperature
624 impact on ice shelf extent in the eastern Antarctic Peninsula, Nat. Commun. 10, 1-8,
625 https://doi.org/10.1038/s41467-018-08195-6, 2019.

626 Evans, T. W., Wormer, L., Lever, M. A., Lipp, J. S., Lagostina, L., Lin, Y. S., Jorgensen, B. B. and Hinrichs,
627 K. U.: Size and composition of subseafloor microbial community in the Benguela upwelling area examined
628 from intact membrane lipid and DNA analysis, Org. Geochem., 111, 86–100,
629 https://doi.org/10.1016/j.orggeochem.2017.06.008, 2017.

630 Fietz, S., Huguet, C., Rueda, G., Hambach, B. and Rosell-Melé, A.: Hydroxylated isoprenoidal GDGTs in
631 the Nordic Seas, Mar. Chem., 152, 1–10, https://doi.org/10.1016/j.marchem.2013.02.007, 2013.

632 Fietz, S., Ho, S. L., Huguet, C., Rosell-Mele, A. and Martinez-Garcia, A.: Appraising GDGT-based seawater
633 temperature indices in the Southern Ocean, Org. Geochem., 102, 93–105,
634 https://doi.org/10.1016/j.orggeochem.2016.10.003, 2016.

635 Francis, C. A., Roberts, K. J., Beman, J. M., Santoro, A. E. and Oakley, B. B.: Ubiquity and diversity of
636 ammonia-oxidizing archaea in water columns and sediments of the ocean, Proc. Natl. Acad. Sci. U. S. A.,
637 102, 14683–14688, https://doi.org/10.1073/pnas.0506625102, 2005.

638 Freeman, N. M., Munro, D. R., Sprintall, J., Mazloff, M. R., Purkey, S., Rosso, I., DeRanek, C. A. and
639 Sweeney, C.: The observed seasonal cycle of macronutrients in Drake Passage: Relationship to fronts and
640 utility as a model metric, J. Geophys. Res. Oceans, 124, 4763–4783, https://doi.org/10.1029/2019JC015052,
641 2019.

642 Gerringa, L. J. A., Alderkamp, A.-C., Laan, P., Thuroczy, C.-E., De Baar, H. J. W., Mills, M. M., van
643 Dijken, G. L., van Haren, H. and Arrigo, K. R.: Iron from melting glaciers fuels the phytoplankton blooms in
644 Amundsen Sea (Southern Ocean): Iron biogeochemistry, Deep-Sea Res. Part II- Top. Stud. Oceanogr., 71–
645 76, 16–31, https://doi.org/10.1016/j.dsr2.2012.03.007, 2012.

646 Gohl, K.: The Expedition PS104 of the Research Vessel POLARSTERN to the Amundsen Sea in 2017,
647 Alfred-Wegener-Institut, Helmholtz-Zentrum für Polar- und Meeresforschung;, Bremerhaven, Germany,
648 https://doi.org/10.2312/BzPM_0712_2017, 2017.

649 Hallam, S. J., Mincer, T. J., Schleper, C., Preston, C. M., Roberts, K., Richardson, P. M. and DeLong, E. F.:
650 Pathways of carbon assimilation and ammonia oxidation suggested by environmental genomic analyses of
651 marine Crenarchaeota, Plos Biol., 4, 520–536, https://doi.org/10.1371/journal.pbio.0040095, 2006.

652 Hernandez, E.A., Piquet, A.M.T., Lopez, J.L., Buma, A.G.J. and Mac Cormack, W.P.: Marine archaeal
653 community structure from Potter Cove, Antarctica: high temporal and spatial dominance of the phylum
654 Thaumarchaeota, Polar. Biol., 38, 117-130, https://doi.org/10.1007/s00300-014-1569-8, 2015

655 Heywood, K. J., Garabato, A. C. N. and Stevens, D. P.: High mixing rates in the abyssal Southern Ocean,
656 Nature, 415, 1011–1014, https://doi.org/10.1038/4151011a, 2002.

657 Hillenbrand, C.-D., Smith, J.A., Hodell, D.A., Greaves, M., Poole, C.R., Kender, S., Williams, M.,
658 Andersen, T.J., Jernas, P.E., Elderfield, H., Klages, J.P., Roberts, S.J., Gohl, K., Larter, R.D. and Kuhn, G.:
659 West Antarctic Ice Sheet retreat driven by Holocene warm water incursions, Nature 547, 43-48
660 https://doi.org/10.1038/nature22995, 2017.

661 Ho, S. L., Mollenhauer, G., Feitz, S., Martinez-Garcia, A., Lamy, F., Rueda, G., Schipper, K., Méheust, M.,
662 Rosell-Melé, Stein, R. and Tiedemann, R.: Appraisal of TEX86 and TEX86L thermometries in subpolar and
663 polar regions, Geochim. Cosmochim. Acta., 131, 213-226, https://doi.org/ 10.1016/j.gca.2014.01.001, 2014.

https://doi.org/10.5194/bg-2020-333
Preprint. Discussion started: 5 November 2020

664 Ho, S. L., Yamamoto, M., Mollenhauer, G. and Minagawa, M.: Core top TEX86 values in the South and
665 equatorial Pacific, Org. Geochem., 42, 94-99, https://doi.org/ 10.1016/j.orggeochem.2010.10.012, 2011.

666 Hu, A. Y., Jiao, N. Z., Zhang, R. and Yang, Z.: Niche partitioning of marine group I Crenarchaeota in the
667 euphotic and upper mesopelagic zones of the East China Sea, Appl. Environ. Microbiol., 77, 7469–7478,
668 https://doi.org/10.1128/Aem.00294-11, 2011.

669 Huguet, C. Kim, J.-H., Sinninghe Damsté, J.S. and Schouten, S.: Reconstruction of sea surface temperature
670 variations in the Arabian Sea over the last 23 kyr using organic proxies (TEX86 and U37K′), Paleoceanogr.
671 Paleoclimatol., 21, PA3003, https://doi.org/10.1029/2005PA001215, 2006.

672 Huguet, C., Urakawa, H., Martens-Habbena, W., Truxal, L., Stahl, D. A. and Ingalls, A. E.: Changes in intact
673 membrane lipid content of archaeal cells as an indication of metabolic status, Org. Geochem., 41, 930–934,
674 https://doi.org/10.1016/j.orggeochem.2010.04.012, 2010.

675 Huguet, C., Martrat, B., Grimalt, J.O., Sinninghe Damsté, J.S. and Schouten, S.: Coherent millennial-scale
676 patterns in U37k′ and TEX86H temperature records during the penultimate interglacial-to-glacial cycle in the
677 western Mediterranean, 26, PA2218, https://doi.org/ 10.1029/2010PA002048, 2011.

678 Huguet, C., Fietz, S. and Rosell-Melé, A.: Global distribution patterns of hydroxy glycerol dialkyl glycerol
679 tetraethers, Org. Geochem., 57, 107–118, https://doi.org/10.1016/j.orggeochem.2013.01.010, 2013.

680 Huguet, C., Fietz, S., Rosell-Mele, A., Daura, X. and Costenaro, L.: Molecular dynamics simulation study of
681 the effect of glycerol dialkyl glycerol tetraether hydroxylation on membrane thermostability, Biochim.
682 Biophys. Acta-Biomembr., 1859, 966–974, https://doi.org/10.1016/j.bbamem.2017.02.009, 2017.

683 Hurley, S. J., Lipp, J. S., Close, H. G., Hinrichs, K. U. and Pearson, A.: Distribution and export of isoprenoid
684 tetraether lipids in suspended particulate matter from the water column of the Western Atlantic Ocean, Org.
685 Geochem., 116, 90–102, https://doi.org/10.1016/j.orggeochem.2017.11.010, 2018.

686 Ingalls, A. E., Shah, S. R., Hansman, R. L., Aluwihare, L. I., Santos, G. H., Druffel, E. R. M. and Pearson,
687 A.: Quantifying archaeal community autotrophy in the mesopelagic ocean using natural radiocarbon, PNAS,
688 103, 6442-6447, https://doi.org/ 10.1073/pnas.0510157103, 2006.

689 Ingalls, A. E, Huguet, C. and Truxal, L.: Distribution of Intact and Core Membrane Lipids of Archaeal
690 Glycerol Dialkyl Glycerol Tetraethers among Size-Fractionated Particulate Organic Matter in Hood Canal,
691 Puget Sound, Appl. Environ. Microbiol., 78, 1480-1490, https://doi.org/ 10.1128/AEM.07016-11, 2012.

692 Jacobs, S. S., Hellmer, H. H. and Jenkins, A.: Antarctic ice sheet melting in the Southeast Pacific, Geophys.
693 Res. Lett., 23, 957–960, https://doi.org/10.1029/96gl00723, 1996.

694 Jacobs, S. S., Jenkins, A., Giulivi, C. F. and Dutrieux, P.: Stronger ocean circulation and increased melting
695 under Pine Island Glacier ice shelf, Nat. Geosci., 4, 519-523, https://doi.org/10.1038/ngeo1188, 2011.

696 Jenkins, A., Dutrieux, P., Jacobs, S. S., McPhail, S. D., Perrett, J. R., Webb, A. T. and White, D.:
697 Observations beneath Pine Island Glacier in West Antarctica and implications for its retreat, Nat. Geosci., 3,
698 468-472, https://doi.org/10.1038/ngeo890, 2010.

699 Jenkyns, H.C., Forster, A., Schouten, S. and Sinninghe Damsté, J.S.: High temperatures in the Late
700 Cretaceous Arctic Ocean, Nature, 432, 888-892, https://doi.org/ 10.1038/nature03143, 2004.

701 Joughin, I., Smith, B. E. and Medley, B.: Marine ice sheet collapse potentially under way for the Thwaites
702 Glacier Basin, West Antarctica, Science, 344, 735–738, https://doi.org/10.1126/science.1249055, 2014.

703 Kalanetra, K. M., Bano, N. and Hollibaugh, J. T.: Ammonia-oxidizing archaea in the Arctic Ocean and
704 Antarctic coastal waters, Environ. Microbiol., 11, 2434–2445, https://doi.org/10.1111/j.1462-
705 2920.2009.01974.x, 2009.

706 Kang, S. J., Shin, K. H. and Kim, J. H.: Occurrence and distribution of hydroxylated isoprenoid glycerol
707 dialkyl glycerol tetraethers (OH-GDGTs) in the Han River system, South Korea, Acta Geochim., 36, 367–
708 369, https://doi.org/10.1007/s11631-017-0165-3, 2017.

709 Kim, J.-G., Park, S.-J., Quan, Z.-X., Jung, M.-Y., Cha, I.-T., Kim, S.-J., Kim, K.-H., Yang, E.-J., Kim, Y.-N.,
710 Lee, S.-H. and Rhee, S.-K.: Unveiling abundance and distribution of planktonic bacteria and archaea in a
711 polynya in Amundsen Sea, Antarctica, Environ. Microbiol., 16, 1566-1578, https://doi.org/ 10.1111/1462-
712 2920.12287. 2014.

713 Kim, J. -H., Schouten, S., Hopmans, E. C., Donner, B. and Sinninghe Damsté, J. S.: Global sediment core-
714 top calibration of the TEX86 paleothermometer in the ocean, Geochim. Cosmochim. Acta, 72, 1154–1173,
715 https://doi.org/10.1016/i.gca.2007.12.010, 2008.

716 Kim, J. -H., van der Meer, J., Schouten, S., Helmke, P., Willmott, V., Sangiorgi, F., Koç, N., Hopmans, E. C.
717 and Sinninghe Damsté, J. S.: New indices and calibrations derived from the distribution of crenarchaeal
718 isoprenoid tetraether lipids: Implications for past sea surface temperature reconstructions, Geochim.
719 Cosmochim. Acta, 74, 4639–4654, https://doi.org/10.1016/j.gca.2010.05.027, 2010.

720 Kim, J.-H., Crosta, X., Willmott, V., Renssen, H., Bonnin, J., Helmke, P., Schouten, S. and Sinninghe
721 Damsté, J. S.: Holocene subsurface temperature variability in the eastern Antarctic continental margin,
722 Geophys. Res. Lett., 39, n/a-n/a, https://doi.org/10.1029/2012gl051157, 2012.

723 Kim, J.-H., Villanueva, L., Zell, C. and Sinninghe Damsté, J. S.: Biological source and provenance of deep-
724 water derived isoprenoid tetraether lipids along the Portuguese continental margin, Geochim. Cosmochim.
725 Acta, 172, 177–204, https://doi.org/10.1016/j.gca.2015.09.010, 2016.

726 Kirchman, D. L., Elifantz, H., Dittel, A. I., Malmstrom, R. R. and Cottrell, M. T.: Standing stocks and
727 activity of Archaea and Bacteria in the western Arctic Ocean, Limnol. Oceanogr., 52, 495–507,
728 https://doi.org/10.4319/lo.2007.52.2.0495, 2007.

729 Lee, S. H., Kang, Y-C. and Fuhrman, J. A.: Imperfect retention of natural bacterioplankton cells by glass
730 fiber filters, Mar. Ecol. Prog. Ser., 119, 285-290, https://doi.org/ 10.3354/meps119285, 1995.

731 Legendre, P., Oksanen, J. and ter Braak, C.J.: Testing the significance of canonical axes in redundancy
732 analysis, Methods Ecol. Evol., 2, 269-277, https://doi.org/ 10.1111/j.2041-210X.2010.00078.x, 2011.

733 Legendre, P. and Legendre, L.: Numerical Ecology, Third Edition, Elsevier, Oxford (UK), ISBN: 978-0-444-
734 53869-7, 2012.

735 Lengger, S. K., Kraaij, M., Tjallingii, R., Baas, M., Stuut, J.-B., Hopmans, E. C., Sinninghe Damsté, J. S.
736 and Schouten, S.: Differential degradation of intact polar and core glycerol dialkyl glycerol tetraether lipids
737 upon post-depositional oxidation, Org. Geochem., 65, 83–93,
738 https://doi.org/https:10.1016/j.orggeochem.2013.10.004, 2013.

739 Lengger, S. K., Hopmans, E. C., Sinninghe Damsté, J. S. and Schouten, S.: Fossilization and degradation of
740 archaeal intact polar tetraether lipids in deeply buried marine sediments (Peru Margin), Geobiology, 12, 212–
741 220, https://doi.org/10.1111/gbi.12081, 2014.

742 Lincoln, S. A., Wai, B., Eppley, J. M., Church, M. J., Summons, R. E. and DeLong, E. F.: Planktonic
743 Euryarchaeota are a significant source of archaeal tetraether lipids in the ocean, Proc. Natl. Acad. Sci. U. S.
744 A., 111, 9858–9863, https://doi.org/10.1073/pnas.1409439111, 2014a.

745 Lincoln, S. A., Wai, B., Eppley, J. M., Church, M. J., Summons, R. E. and DeLong, E. F.: Reply to Schouten
746 et al.: Marine Group II planktonic Euryarchaeota are significant contributors to tetraether lipids in the ocean,
747 Proc. Natl. Acad. Sci. U. S. A., 111, E4286–E4286, https://doi.org/10.1073/pnas.1416736111, 2014b.

748 Lipp, J. S. and Hinrichs, K. U.: Structural diversity and fate of intact polar lipids in marine sediments,
749 Geochim. Cosmochim. Acta, 73, 6816–6833, https://doi.org/10.1016/j.gca.2009.08.003, 2009.

750 Lipp, J. S., Morono, Y., Inagaki, F. and Hinrichs, K. U.: Significant contribution of Archaea to extant
751 biomass in marine subsurface sediments, Nature, 454, 991–994, https://doi.org/10.1038/nature07174, 2008.

752 Liu, X. L., Lipp, J. S., Simpson, J. H., Lin, Y. S., Summons, R. E. and Hinrichs, K. U.: Mono- and
753 dihydroxyl glycerol dibiphytanyl glycerol tetraethers in marine sediments: Identification of both core and
754 intact polar lipid forms, Geochim. Cosmochim. Acta, 89, 102–115,
755 https://doi.org/10.1016/j.gca.2012.04.053, 2012.

756 Locarnini, R. A., Whitworth, T. and Nowlin, W. D.: The importance of the Scotia Sea on the outflow of
757 Weddell Sea Deep-Water, J. Mar. Res., 51, 135–153, https://doi.org/10.1357/0022240933223846, 1993.

758 Lu, X. X., Liu, X. L., Elling, F. J., Yang, H., Xie, S. C., Song, J. M., Li, X. G., Yuan, H. M., Li, N. and
759 Hinrichs, K. U.: Hydroxylated isoprenoid GDGTs in Chinese coastal seas and their potential as a
760 paleotemperature proxy for mid-to-low latitude marginal seas, Org. Geochem., 89–90, 31–43,
761 https://doi.org/10.1016/j.orggeochem.2015.10.004, 2015.

762 Luo, H. W., Tolar, B. B., Swan, B. K., Zhang, C. L. L., Stepanauskas, R., Moran, M. A. and Hollibaugh, J.
763 T.: Single-cell genomics shedding light on marine Thaumarchaeota diversification, Isme J., 8, 732–736,
764 https://doi.org/10.1038/ismej.2013.202, 2014.

765 Mankoff, K. D., Jacobs, S. S., Tulaczyk, S. M. and Stammerjohn, S. E.: The role of Pine Island Glacier ice
766 shelf basal channels in deep-water upwelling, polynyas and ocean circulation in Pine Island Bay, Antarctica,
767 Ann. Glaciol., 53, 123–128, https://doi.org/10.3189/2012AoG60A062, 2012.

768 Massana, R., Taylor, L. J., Murray, A. E., Wu, K. Y., Jeffrey, W. H. and DeLong, E. F.: Vertical distribution
769 and temporal variation of marine planktonic archaea in the Gerlache Strait, Antarctica, during early spring,
770 Limnol. Oceanogr., 43, 607–617, https://doi.org/10.4319/lo.1998.43.4.0607, 1998.

771 Menviel, L., Timmermann, A., Timm, O. E. and Mouchet, A.: Climate and biogeochemical response to a
772 rapid melting of the West Antarctic Ice Sheet during interglacials and implications for future climate,
773 Paleoceanography, 25, https://doi.org/10.1029/2009PA001892, 2010.

774 Merbt, S. N., Stahl, D. A., Casamayor, E. O., Marti, E., Nicol, G. W. and Prosser, J. I.: Differential
775 photoinhibition of bacterial and archaeal ammonia oxidation, Fems Microbiol. Lett., 327, 41–46,
776 https://doi.org/10.1111/j.1574-6968.2011.02457.x, 2012.

777 Meredith, M. P., Naveira Garabato, A. C., Stevens, D. P., Heywood, K. J., and Sanders, R. J.: Deep and
778 Bottom Waters in the Eastern Scotia Sea: Rapid Changes in Properties and Circulation, J. Phys. Oceanogr.,
779 31, 2157-2168, https://doi.org/10.1175/1520-0485(2001)031<2157:DABWIT>2.0.CO;2, 2001.

780 Mincer, T. J., Church, M. J., Taylor, L. T., Preston, C., Kar, D. M. and DeLong, E. F.: Quantitative
781 distribution of presumptive archaeal and bacterial nitrifiers in Monterey Bay and the North Pacific
782 Subtropical Gyre, Environ. Microbiol., 9, 1162–1175, https://doi.org/10.1111/j.1462-2920.2007.01239.x,
783 2007.

784 Mouginot, J., Rignot, E. and Scheuchl, B.: Sustained increase in ice discharge from the Amundsen Sea
785 Embayment, West Antarctica, from 1973 to 2013, Geophys. Res. Lett., 41, 1576-1584, https://doi.org/
786 10.1002/2013GL059069, 2014.

787 Murray, A. E., Preston, C. M., Massana, R., Taylor, L. T., Blakis, A., Wu, K. and DeLong, E. F.: Seasonal
788 and spatial variability of bacterial and archaeal assemblages in the coastal waters near Anvers Island,
789 Antarctica, Appl. Environ. Microbiol., 64, 2585–2595, https://doi.org/ 10.1128/AEM.64.7.2585-2595, 1998.

790 Naveira Garabato, A. C., Heywood, K. J. and Stevens, D. P.: Modification and pathways of Southern Ocean
791 Deep Waters in the Scotia Sea, Deep Sea Res. Part I Oceanogr. Res. Pap., 49, 681-705, https://doi.org/
792 10.1016/S0967-0637(01)00071-1, 2002a.

793 Naveira Garabato, A. C., Strass, V. H. and Kattner, G.: Fluxes of nutrients in a three-dimensional meander
794 structure of the Antarctic Polar Front, Deep Sea Res. Part II Top. Stud. Oceanogr., 49, 3771-3792,
795 https://doi.org/10.1016/S0967-0645(02)00110-8, 2002b.

796 Orsi, A. H., Whitworth, T. and Nowlin Jr., W. D.: On the meridional extent and fronts of the Antarctic
797 Circumpolar Current, Deep Sea Res. Part I Oceanogr. Res. Pap., 42, 641-673, https://doi.org/10.1016/0967-
798 0637(95)00021-W, 1995.

799 Paolo, F. S., Fricker, H. A. and Padman, L.: Volume loss from Antarctic ice shelves is accelerating, Science,
800 348, 327-331, https://doi.org/10.1126/science.aaa0940, 2015.

801 Park, J., Kuzminov, F. I., Bailleul, B., Yang, E. J., Lee, S., Falkowski, P. G. and Gorbunov, M. Y.: Light
802 availability rather than Fe controls the magnitude of massive phytoplankton bloom in the Amundsen Sea
803 polynyas, Antarctica, Limnol. Oceanogr., 62, 2260–2276, https://doi.org/10.1002/lno.10565, 2017.

804 Pitcher, A., Rychlik, N., Hopmans, E. C., Spieck, E., Rijpstra, W. I. C., Ossebaar, J., Schouten, S., Wagner,
805 M. and Sinninghe Damsté, J. S.: Crenarchaeol dominates the membrane lipids of "*Candidatus*
806 *Nitrososphaera gargensis*", a thermophilic Group I. 1b Archaeon, Isme J., 4, 542–552,
807 https://doi.org/10.1038/ismej.2009.138, 2010.

808 Pitcher, A., Hopmans, E. C., Mosier, A. C., Park, S. J., Rhee, S. K., Francis, C. A., Schouten, S. and
809 Sinninghe Damsté, J. S.: Core and Intact Polar Glycerol Dibiphytanyl Glycerol Tetraether Lipids of
810 Ammonia-Oxidizing Archaea Enriched from Marine and Estuarine Sediments, Appl. Environ. Microbiol.,
811 77, 3468–3477, https://doi.org/10.1128/Aem.02758-10, 2011.

812 Pritchard, H. D., Arthern, R. J., Vaughan, D. G. and Edwards, L. A.: Extensive dynamic thinning on the
813 margins of the Greenland and Antarctic ice sheets, Nature, 461, 971–975,
814 https://doi.org/10.1038/nature08471, 2009.

815 Raes, E. J., Bodrossy, L., van de Kamp, J., Bissett, A., Ostrowski, M., Brown, M. V., Sow, S. L. S., Sloyan,
816 B. and Waite, A. M.: Oceanographic boundaries constrain microbial diversity gradients in the South Pacific
817 Ocean, Proc. Natl. Acad. Sci., 115, E8266–E8275, https://doi.org/10.1073/pnas.1719335115, 2018.

818 Raiswell, R., Benning, L. G., Tranter, M. and Tulaczyk, S.: Bioavailable iron in the Southern Ocean: the
819 significance of the iceberg conveyor belt, Geochem. Trans., 9, https://doi.org/10.1186/1467-4866-9-7, 2008.

820 Rignot, E. and Jacobs, S. S.: Rapid bottom melting widespread near Antarctic ice sheet grounding lines,
821 Science, 296, 2020–2023, https://doi.org/10.1126/science.1070942, 2002.

822 Rignot, E., Bamber, J. L., Van Den Broeke, M. R., Davis, C., Li, Y. H., Van De Berg, W. J. and Van
823 Meijgaard, E.: Recent Antarctic ice mass loss from radar interferometry and regional climate modelling, Nat.
824 Geosci., 1, 106–110, https://doi.org/10.1038/ngeo102, 2008.

825 Rignot, E., Jacobs, S., Mouginot, J. and Scheuchl, B.: Ice-Shelf Melting Around Antarctica, Science, 341,
826 266–270, https://doi.org/10.1126/science.1235798, 2013.

827 Rignot, E., Mouginot, J., Scheuchl, B., Van Den Broeke, M., Van Wessem, M.J. and Morlighem, M.: Four
828 decades of Antarctic ice sheet mass balance from 1979-2017, PNAS, 116, 1095-1103, https://doi.org/
829 10.1073/pnas.1812883116, 2019.

830 Rubin, S. I.: Carbon and nutrient cycling in the upper water column across the Polar Frontal Zone and
831 Antarctic Circumpolar Current along 170°W, Glob. Biogeochem. Cycles, 17, 1-14,
832 https://doi.org/10.1029/2002GB001900, 2003.

833 Schouten, S., Hopmans, E. C., Pancost, R. D. and Sinninghe Damsté, J. S.: Widespread occurrence of
834 structurally diverse tetraether membrane lipids: Evidence for the ubiquitous presence of low-temperature
835 relatives of hyperthermophiles, Proc. Natl. Acad. Sci. U. S. A., 97, 14421–14426,
836 https://doi.org/10.1073/pnas.97.26.14421, 2000.

837 Schouten, S., Hopmans, E. C., Schefuß, E. and Sinninghe Damsté, J. S.: Distributional variations in marine
838 crenarchaeotal membrane lipids: a new tool for reconstructing ancient sea water temperatures?, Earth Planet.
839 Sci. Lett., 204, 265–274, https://doi.org/10.1016/S0012-821X(02)00979-2, 2002.

840 Schouten, S., Huguet, C., Hopmans, E. C., Kienhuis, M. V. M. and Sinninghe Damsté, J. S.: Analytical
841 methodology for TEX86 paleothermometry by high-performance liquid chromatography/atmospheric
842 pressure chemical ionization-mass spectrometry, Anal. Chem., 79, 2940–2944,
843 https://doi.org/10.1021/ac062339v, 2007.

844 Schouten, S., Baas, M., Hopmans, E. C., Reysenbach, A. L. and Sinninghe Damsté, J. S.: Tetraether
845 membrane lipids of Candidatus "*Aciduliprofundum boonei*", a cultivated obligate thermoacidophilic

euryarchaeote from deep-sea hydrothermal vents, Extremophiles, 12, 119–124, https://doi.org/10.1007/s00792-007-0111-0, 2008.

Schouten, S., Middelburg, J. J., Hopmans, E. C. and Sinninghe Damsté, J. S.: Fossilization and degradation of intact polar lipids in deep subsurface sediments: A theoretical approach, Geochim. Cosmochim. Acta, 74, 3806–3814, https://doi.org/10.1016/j.gca.2010.03.029, 2010.

Schouten, S., Pitcher, A., Hopmans, E. C., Villanueva, L., van Bleijswijk, J. and Sinninghe Damsté, J. S.: Intact polar and core glycerol dibiphytanyl glycerol tetraether lipids in the Arabian Sea oxygen minimum zone: I. Selective preservation and degradation in the water column and consequences for the TEX86, Geochim. Cosmochim. Acta, 98, 228–243, https://doi.org/10.1016/j.gca.2012.05.002, 2012.

Schouten, S., Hopmans, E. C. and Sinninghe Damsté, J. S.: The organic geochemistry of glycerol dialkyl glycerol tetraether lipids: A review, Org. Geochem., 54, 19–61, https://doi.org/10.1016/j.orggeochem.2012.09.006, 2013.

Schouten, S., Villanueva, L., Hopmans, E. C., van der Meer, M. T. J. and Sinninghe Damsté, J. S.: Are Marine Group II Euryarchaeota significant contributors to tetraether lipids in the ocean?, Proc. Natl. Acad. Sci. U. S. A., 111, 4285, https://doi.org/10.1073/pnas.1416176111, 2014.

Schubotz, F., Wakeham, S. G., Lipp, J. S., Fredricks, H. F. and Hinrichs, K. U.: Detection of microbial biomass by intact polar membrane lipid analysis in the water column and surface sediments of the Black Sea, Environ. Microbiol., 11, 2720–2734, https://doi.org/10.1111/j.1462-2920.2009.01999.x, 2009.

Shah, S. R., Mollenhauer, G., Ohkouchi, N., Eglinton, T. I. and Pearson, A.: Origins of archaeal tetrarther lipids in sediments: Insights from radiocarbon analysis, Geochim. Cosmochim. Acta., 72, 4577-4594, https://doi.org/ 10.1016/j.gca.2008.06.021, 2008.

Shepherd, A., Wingham, D. J., Mansley, J. A. D. and Corr, H. F. J.: Inland thinning of Pine Island Glacier, West Antarctica, Science, 291, 862–864, https://doi.org/10.1126/science.291.5505.862, 2001.

Shevenell, A.E., Ingalls, A.E., Dormack, E.W. and Kelly, C.: Holocene Southern Ocean surface temperature variability west of the Antarctic Peninsula. Nature, 470, 250-254, https://doi.org/10.1038/nature09751, 2011.

871 Signori, C.N., Pellizari, V.H., Enrich-Prast, A. and Sievert, S.M.: Spatiotemporal dynamics of marine
872 bacterial and archaeal communities in surface waters off the northern Antarctic Peninsula, Deep Sea Res.
873 Part II Top. Stud. Oceanogr., 149, 150-160, https://doi.org/ 10.1016/j.dsr2.2017.12.017, 2018.

874 Sinninghe Damsté, J.S., van Bentum, E.C., Reichart, G-J., Pross, J. and Schouten, S.: A CO2 decrease-driven
875 cooling and increased latitudinal temperature gradient during the mid-Cretaceous Oceanic Anoxic Event 2,
876 Earth Planet. Sci. Lett. 293, 97-103, https://doi.org/ 10.1016/j.epsl.2010.02.027, 2010.

877 Sinninghe Damsté, J. S., Rijpstra, W. I. C., Hopmans, E. C., Jung, M. Y., Kim, J. G., Rhee, S. K.,
878 Stieglmeier, M. and Schleper, C.: Intact polar and core Glycerol Dibiphytanyl Glycerol Tetraether lipids of
879 Group I.1a and I.1b Thaumarchaeota in soil, Appl. Environ. Microbiol., 78, 6866–6874,
880 https://doi.org/10.1128/aem.01681-12, 2012.

881 Sinninghe Damsté, J. S., Rijpstra, W. I. C., Hopmans, E. C., den Uijl, M.J., Weijers, J.W.H., Schouten, S.
882 The enigmatic structure of the crenarchaeol isomer, Org. Geochem., 124, 22-28,
883 https://doi.org/10.1016/j.orggeochem.2018.06.005, 2018.

884 Smith, J.A., Andersen, T.J., Shortt, M., Truffer, M., Stanton, T.P., Bindschadler, R., Dutrieux, P., Jenkins,
885 A., Hillenbrand, C.-D., Ehrmann, W., Corr, H.F.J., Farley, N., Crowhurst, S. and Vaughan, D.G.: Sub-ice-
886 shelf sediments record history of 20th Century retreat of Pine Island Glacier. Nature 540, 77-80,
887 https://doi.org/10.1038/nature20136. 2017.

888 Sokolov, S. and Rintoul, S. R.: Circulation structure and distribution of the Antarctic Circumpolar Current
889 fronts: 1. Mean circumpolar paths. J. Geophys.Res. 114, C11018, https://doi.org/ 10.1029/2008JC005248.
890 2009.

891 Sollai, M., Villanueva, L., Hopmans, E.C., Reichart, G-J., Sinninghe Damsté, J.S.: A combined lipidomic
892 and 16S rRNA gene amplicon sequencing approach reveals archaeal sources of intact polar lipids in the
893 stratified Black Sea water column, Geobiology., 17, 91-109, https://doi.org/ 10.1111/gbi.12316, 2019a.

894 Sollai, M., Villanueva, L., Hopmans, E.C., Keil, R.G., Sinninghe Damsté, J.S.: Archaeal sources of intact
895 membrane lipid biomarkers in the oxygen deficient zone of the Eastern Tropical South Pacific, Front.
896 Microbiol., 10, https://doi.org/ 10.3389/fmicb.2019.00765, 2019b.

897 Sollich, M., Yoshinaga, M. Y., Hausler, S., Price, R. E., Hinrichs, K. U. and Buhring, S. I.: Heat stress
898 dictates microbial lipid composition along a thermal gradient in marine sediments, Front. Microbiol., 8, 1-19
899 https://doi.org/10.3389/fmicb.2017.01550, 2017.

900 Spang, A., Hatzenpichler, R., Brochier-Armanet, C., Rattei, T., Tischler, P., Spieck, E., Streit, W., Stahl, D.
901 A., Wagner, M. and Schleper, C.: Distinct gene set in two different lineages of ammonia-oxidizing archaea
902 supports the phylum Thaumarchaeota, Trends Microbiol., 18, 331–340,
903 https://doi.org/10.1016/j.tim.2010.06.003, 2010.

904 St-Laurent, P., Yager, P. L., Sherrell, R. M., Stammerjohn, S. E. and Dinniman, M. S.: Pathways and supply
905 of dissolved iron in the Amundsen Sea (Antarctica), J. Geophys. Res. Oceans, 122, 7135–7162,
906 https://doi.org/10.1002/2017JC013162, 2017.

907 Sturt, H. F., Summons, R. E., Smith, K., Elvert, M. and Hinrichs, K. U.: Intact polar membrane lipids in
908 prokaryotes and sediments deciphered by high-performance liquid chromatography/electrospray ionization
909 multistage mass spectrometry - new biomarkers for biogeochemistry and microbial ecology, Rapid Commun.
910 Mass Spectrom., 18, 617–628, https://doi.org/10.1002/rcm.1378, 2004.

911 Thuroczy, C.-E., Alderkamp, A.-C., Laan, P., Gerringa, L. J. A., Mills, M. M., Van Dijken, G. L., De Baar,
912 H. J. W. and Arrigo, K. R.: Key role of organic complexation of iron in sustaining phytoplankton blooms in
913 the Pine Island and Amundsen Polynyas (Southern Ocean), Deep-Sea Res. Part II- Top. Stud. Oceanogr., 71–
914 76, 49–60, https://doi.org/10.1016/j.dsr2.2012.03.009, 2012.

915 Tolar, B. B., Ross, M. J., Wallsgrove, N. J., Liu, Q., Aluwihare, L. I., Popp, B. N. and Hollibaugh, J. T.:
916 Contribution of ammonia oxidation to chemoautotrophy in Antarctic coastal waters, Isme J., 10, 2605–2619,
917 https://doi.org/10.1038/ismej.2016.61, 2016.

918 Venables, H. J.: JR272A Weddell and Scotia Sea hydrographic section, British Antarctic Survey, Cambridge,
919 UK, https://www.bodc.ac.uk/resources/inventories/cruise_inventory/reports/jr272.pdf, 2012.

920 Vernet, M., Geibert, W., Hoppema, M., Brown, P. J., Haas, C., Hellmer, H. H., Jokat, W., Jullion, L.,
921 Mazloff, M., Bakker, D. C. E., Brearley, J. A., Croot, P., Hattermann, T., Hauck, J., Hillenbrand, C-D.,
922 Hoppe, C. J. M., Huhn, O., Koch, B. P., Lechtenfeld, O. J., Meredith, M. P., Naveira Garabato, A. C.,
923 Nöthig, E.-M., Peeken, I., Rutgers van der Loeff, M. M., Schmidtko, S., Schröder, M., Strass, V. H., Torres-

924 Valdés, S. and Verdy, A.: The Weddell Gyre, Southern Ocean: Present knowledge and future challenges,
925 Rev. Geophys. 57, 623-708, https://doi.org/10.1029/2018RG000604, 2019.

926 Wadham, J. L., De'ath, R., Monteiro, F. M., Tranter, M., Ridgwell, A., Raiswell, R. and Tulaczyk, S.: The
927 potential role of the Antarctic Ice Sheet in global biogeochemical cycles, Earth Environ. Sci. Trans. R. Soc.
928 Edinb., 104, 55–67, https://doi.org/10.1017/S1755691013000108, 2013.

929 Wadham, J. L., Hawkings, J. R., Tarasov, L., Gregoire, L. J., Spencer, R. G. M., Gutjahr, M., Ridgwell, A.
930 and Kohfeld, K. E.: Ice sheets matter for the global carbon cycle., Nat. Commun., 10, 1-17, https://doi.org/
931 10.1038/s41467-019-11394-4, 2019.

932 Webber, B. G. M., Heywood, K. J., Stevens, D. P., Dutrieux, P., Abrahamsen, E. P., Jenkins, A., Jacobs, S.
933 S., Ha, H. K., Lee, S. H., and Kim, T. W.: Mechanisms driving variability in the ocean forcing of Pine Island
934 Glacier, Nat. Commun., 8, https://doi.org/ 14507, 10.1038/ncomms14507, 2017.

935 Wilkins, D., Lauro, F. M., Williams, T. J., Demaere, M. Z., Brown, M. V., Hoffman, J. M., Andrews-
936 Pfannkoch, C., Mcquaid, J. B., Riddle, M. J., Rintoul, S. R. and Cavicchioli, R.: Biogeographic partitioning
937 of Southern Ocean microorganisms revealed by metagenomics, Environ. Microbiol., 15, 1318–1333,
938 https://doi.org/10.1111/1462-2920.12035, 2013.

939 Wingham, D. J., Wallis, D. W. and Shepherd, A.: Spatial and temporal evolution of Pine Island Glacier
940 thinning, 1995-2006, Geophys. Res. Lett., 36, 1-5, https://doi.org/10.1029/2009gl039126, 2009.

941 Xie, S. T., Lipp, J. S., Wegener, G., Ferdelman, T. G. and Hinrichs, K-U.: Turnover of microbial lipid in the
942 deep biosphere and growth of benthic archaeal populations, PNAS, 100, 6010-6014, https://doi.org/
943 10.1073/pnas.1218569110, 2013.

944 Xie, S. T., Liu, X. L., Schubotz, F., Wakeham, S. G. and Hinrichs, K. U.: Distribution of glycerol ether lipids
945 in the oxygen minimum zone of the Eastern Tropical North Pacific Ocean, Org. Geochem., 71, 60–71,
946 https://doi.org/10.1016/j.orggeochem.2014.04.006, 2014.

947 Yager, P.L., Sherrell, R.M., Stammerjohn, S.E., Alderkamp, A.-C., Schofield, O., Abrahamsen, E.P., Arrigo,
948 K.R., Bertilsson, S., Garay, D.L., Guerrero, R., Lowry, K.E., Moksnes, P.-O., Ndungu, K., Post, A.F.,
949 Randall-Goodwin, E., Riemann, L., Severmann, S., Thatje, S., van Dijken, G.L. and Wilson, S.: ASPIRE:

https://doi.org/10.5194/bg-2020-333
Preprint. Discussion started: 5 November 2020

950 The Amundsen sea Polynya international research expedition. Oceanography, 25, 40-53, https://doi.org/
951 10.5670/oceanog.2012.73. 2012.

952 Zeng, Z., Liu, X-L., Farley, K. R., Wei, J. H., Metcalf, W. W., Summons, R. E. and Welander, P. V.: GDGT
953 cyclization proteins identify the dominant archaeal sources of tetrarther lipids in the ocean. PNAS, 45,
954 22505-22511, https://doi.org/ 10.1073/pnas.1909306116. 2019.

955 Zhang, Y. G., Pagani, M. and Zhengrong, W.: Ring Index: A new strategy to evaluate the integrity of TEX86
956 paleothermometry. Paleoceanography, 31, 220-232, https://doi.org/ 10.1002/2015PA002848. 2016.

957 Zhu, C., Wakeham, S. G., Elling, F. J., Basse, A., Mollenhauer, G., Versteegh, G. J. M., Konneke, M. and
958 Hinrichs, K. U.: Stratification of archaeal membrane lipids in the ocean and implications for adaptation and
959 chemotaxonomy of planktonic archaea, Environ. Microbiol., 18, 4324–4336, https://doi.org/10.1111/1462-
960 2920.13289, 2016.

961 Zwally, H. J., Giovinetto, M. B., Li, J., Cornejo, H. G., Beckley, M. A., Brenner, A. C., Saba, J. L. and Yi,
962 D. H.: Mass changes of the Greenland and Antarctic ice sheets and shelves and contributions to sea-level
963 rise: 1992-2002, J. Glaciol., 51, 509–527, https://doi.org/10.3189/172756505781829007, 2005.

https://doi.org/10.5194/bg-2020-333
Preprint. Discussion started: 5 November 2020

964 Table 1: Scotia Sea SPM samples studied and their physical properties including sample depth (m) and
965 sample layer where "M" denotes mixed layer and "T" denotes thermocline layer (figures to 2 decimal places
966 (d.p.).

Latitude (°N)	Longitude (°E)	Station	Sample Depth (m)	Layer	Temperature (°C)	Salinity (PSU)	Fluorescence (ml/m^3)
-53.013	-58.04	CTD 1	15	M	7.31	33.99	0.41
-53.013	-58.04	CTD 1	100	T	6.12	34.03	0.13
-53.586	-42.835	CTD 23	20	M	4.07	33.72	0.32
-53.586	-42.835	CTD 23	100	T	2.23	33.81	0.08
-52.88	-41.787	CTD 24	15	M	3.55	33.72	1.09
-52.88	-41.787	CTD 24	80	T	1.67	33.88	0.09
-53.743	-38.155	CTD 25	10	M	3.17	33.62	0.66
-53.743	-38.155	CTD 25	80	T	1.95	33.91	0.05
-57.119	-31.815	CTD 22	30	M	1.34	33.82	0.24
-56.167	-34.816	CTD 22	110	T	0.84	34.12	0.09
-57.459	-31.327	CTD 21	30	M	1.48	33.85	0.27
-57.459	-31.327	CTD 21	110	T	1.34	34.3	0.03
-57.803	-30.83	CTD 20	30	M	1.60	33.92	0.28
-57.803	-30.83	CTD 20	110	T	1.01	34.15	0.06
-58.213	-30.822	CTD 19	20	M	1.29	33.9	0.27
-58.213	-30.822	CTD 19	80	T	1.16	34.19	0.09
-58.624	-30.821	CTD 18	20	M	0.65	33.69	0.17
-58.624	-30.821	CTD 18	90	T	-0.83	33.99	0.17
-59.436	-30.861	CTD 16	20	M	-0.64	33.67	0.17
-59.436	-30.861	CTD 16	70	T	-1.32	34.12	0.08
-60.319	-30.961	CTD 13	30	M	-0.89	33.74	0.11
-60.319	-30.961	CTD 13	65	T	-1.16	34.01	0.11
-61.171	-31.045	CTD 10	30	M	-1.08	33.82	0.15
-61.171	-31.045	CTD 10	80	T	-1.08	34.23	0.11
-62.084	-31.174	CTD 7	40	M	-1.11	33.87	0.4
-62.084	-31.174	CTD 7	75	T	-1.54	34.33	0.16
-62.784	-30.706	CTD 5	20	M	-1.13	33.87	0.28
-62.784	-30.706	CTD 5	70	T	-1.49	34.34	0.14
-63.346	-29.569	CTD 3	20	M	-1.18	33.8	0.22
-63.346	-29.569	CTD 3	60	T	-1.58	34.31	0.21

967

https://doi.org/10.5194/bg-2020-333
Preprint. Discussion started: 5 November 2020

968 Table 2: Amundsen Sea SPM samples studied and their physical properties (figures to 2 d.p)

Latitude (° N)	Longitude (°E)	Station	Sample Depth (m)	Temperature (°C)	Salinity (PSU)	Fluorescence (ml/m^3)
-74.958	-101.829	PS104/003-1	10	-0.72	33.96	0.48
-74.958	-101.829	PS104/003-1	120	-1.19	34.13	0.01
-74.958	-101.829	PS104/003-1	180	-1.23	34.17	0.01
-74.958	-101.829	PS104/003-1	998	1.01	34.67	-0.02
-74.866	-100.76	PS104/007-1	20	-0.12	33.52	3.78
-74.866	-100.76	PS104/007-1	120	-0.91	34.08	0.01
-74.866	-100.76	PS104/007-1	240	-1.33	34.14	-0.01
-74.866	-100.76	PS104/007-1	685	0.87	34.63	-0.02
-74.359	-101.747	PS104/017-1	10	-0.17	33.42	7.89
-74.359	-101.747	PS104/017-1	150	-1.61	34.16	0.01
-74.359	-101.747	PS104/017-1	1375	1.06	34.71	-0.02
-72.768	-107.093	PS104/022-1	10	-0.59	33.13	1.09
-72.768	-107.093	PS104/022-1	30	-0.47	33.27	1.71
-72.768	-107.093	PS104/022-1	120	-1.54	34.1	0.07
-72.768	-107.093	PS104/022-1	697	0.98	34.71	-0.02
-73.297	-112.328	PS104/043-2	10	-1.34	32.82	1.51
-73.297	-112.328	PS104/043-2	120	-1.62	34.18	0.01
-73.297	-112.328	PS104/043-2	454	0.15	34.51	-0.02

969

https://doi.org/10.5194/bg-2020-333
Preprint. Discussion started: 5 November 2020

970 Table 3: Relative abundances (%) and heat map of IPLs identified in Scotia Sea. Relative abundances >30%

971 indicated in red, low relative abundances <10% indicated in green. nd = not detected.

CTD	Depth (m)	GDGT-0 MH	GDGT-0 DH	GDGT-0 HPH	GDGT-1 DH	Crenarchaeol MH	Crenarchaeol DH	Crenarchaeol HPH	OH-GDGT-0 MH	OH-GDGT-0 DH	OH-GDGT-0 HPH	diOH-GDGT-0 MH
1	15	6.8	nd	49.6	nd	3.4	nd	18.6	nd	21.6	nd	nd
1	100	4.6	nd	54.9	nd	3.3	nd	5.6	2.6	28.2	nd	0.8
23	20	nd	nd	nd	nd	nd	nd	nd	nd	nd	nd	nd
23	100	31.0	nd	nd	nd	16.8	nd	nd	19.6	17.7	nd	14.9
24	15	nd	nd	nd	nd	nd	nd	nd	nd	nd	nd	nd
24	80	36.2	nd	1.6	nd	23.3	nd	nd	16.5	15.7	nd	6.7
25	10	nd	nd	nd	nd	nd	nd	nd	nd	nd	nd	nd
25	80	10.1	1.0	35.3	nd	6.1	nd	13.4	8.7	14.8	1.8	8.8
22	30	nd	nd	nd	nd	nd	nd	nd	nd	nd	nd	nd
22	110	13.5	nd	8.8	nd	11.9	nd	nd	21.7	23.7	nd	20.4
21	30	52.6	nd	nd	nd	nd	nd	nd	47.4	nd	nd	nd
21	110	9.3	4.0	10.2	3.5	4.5	nd	nd	11.8	35.3	nd	21.4
20	30	53.0	nd	nd	nd	24.5	nd	nd	22.5	nd	nd	nd
20	110	9.0	nd	31.8	nd	6.0	nd	nd	12.4	28.2	nd	12.6
19	20	nd	nd	nd	nd	nd	nd	nd	nd	nd	nd	nd
19	80	3.1	nd	55.7	nd	2.6	nd	4.8	6.4	19.2	nd	8.2
18	20	nd	nd	nd	nd	nd	nd	nd	nd	nd	nd	nd
18	90	4.2	nd	57.8	nd	1.9	nd	13.4	4.7	9.2	2.6	6.2
16	20	nd	nd	100.0	nd	nd	nd	nd	nd	nd	nd	nd
16	70	7.8	nd	45.9	nd	3.2	nd	nd	20.6	8.9	nd	13.6
13	30	nd	nd	nd	nd	nd	nd	nd	nd	nd	nd	nd
13	65	15.3	nd	54.2	nd	4.1	nd	11.1	10.5	nd	nd	4.8
10	30	nd	nd	nd	nd	nd	nd	nd	nd	nd	nd	nd
10	80	4.2	nd	82.6	nd	0.5	nd	nd	7.0	nd	nd	5.7
7	40	nd	nd	nd	nd	nd	nd	nd	nd	nd	nd	nd
7	75	7.2	nd	47.7	nd	2.5	nd	nd	29.8	nd	nd	12.7
5	20	nd	nd	nd	nd	nd	nd	nd	nd	nd	nd	nd
5	70	0.7	nd	71.1	nd	0.4	nd	16.3	2.3	4.8	2.5	1.9
3	20	nd	nd	nd	nd	nd	nd	nd	nd	nd	nd	nd
3	60	45.2	nd	22.7	nd	6.9	nd	nd	25.2	nd	nd	nd

972

https://doi.org/10.5194/bg-2020-333
Preprint. Discussion started: 5 November 2020

Biogeosciences Discussions Open Access EGU

973 Table 4: Relative abundances (%) and heat map of IPLs identified in Amundsen Sea. Relative abundances

974 >30% indicated in red, low relative abundances <10% indicated in green. nd = not detected.

		GDGT-0			GDGT-1	GDGT-2	Crenarchaeol			OH-GDGT-0			diOH-GDGT-0
Station	Depth (cm)	MH	DH	HPH	DH	DH	MH	DH	HPH	MH	DH	HPH	MH
PS104/003-1	10	1.2	nd	81.8	nd	nd	0.2	nd	11.1	0.4	5.1	nd	0.2
PS104/003-1	120	0.6	2.2	56.2	1.5	nd	0.3	0.1	11.7	4.9	16.5	0.5	5.5
PS104/003-1	180	1.4	nd	18.0	nd	nd	0.7	nd	nd	24.1	25.7	nd	30.1
PS104/003-1	998	3.4	11.3	28.1	14.7	8.2	1.7	3.0	4.3	5.2	18.8	nd	1.3
PS104/007-1	20	89.1	nd	nd	nd	nd	10.9	nd	nd	nd	nd	nd	nd
PS104/007-1	120	1.4	4.6	38.8	5.1	1.9	1.0	0.4	7.7	6.9	25.7	nd	6.5
PS104/007-1	240	2.3	5.7	40.0	3.3	nd	1.3	nd	8.3	11.8	11.9	nd	15.4
PS104/007-1	685	1.3	8.9	37.8	9.1	4.1	1.3	1.8	8.3	3.6	22.7	nd	1.1
PS104/017-1	10	nd	nd	nd	nd	nd	nd	nd	nd	nd	nd	nd	nd
PS104/017-1	150	1.7	nd	43.9	nd	nd	1.0	nd	6.8	14.1	13.0	nd	19.5
PS104/017-1	1375	0.9	6.5	38.2	11.1	7.3	1.1	3.0	11.9	2.4	17.3	nd	0.3
PS104/022-1	10	nd	nd	nd	nd	nd	nd	nd	nd	nd	nd	nd	nd
PS104/022-1	30	nd	nd	nd	nd	nd	nd	nd	nd	nd	nd	nd	nd
PS104/022-1	120	2.8	nd	51.6	nd	nd	1.7	nd	12.4	11.1	9.3	1.2	9.9
PS104/022-1	697	4.3	6.0	31.5	11.2	5.3	2.0	2.3	5.6	5.5	25.0	nd	1.2
PS104/043-2	10	nd	nd	nd	nd	nd	nd	nd	nd	nd	nd	nd	nd
PS104/043-2	120	1.6	nd	38.3	nd	nd	0.5	nd	11.5	4.6	37.9	0.9	4.7
PS104/043-2	454	0.7	0.2	72.3	nd	nd	0.2	nd	13.2	1.7	8.6	0.7	2.4

975

https://doi.org/10.5194/bg-2020-333
Preprint. Discussion started: 5 November 2020

976 Table 5: Ratios of monohexose/dihexose (MH/DH), monohexose/hexosephosphohexose (MH/HPH), GDGT-
977 0/crenarchaeol (GDGT-0/Cren), and Ring Index in the Scotia Sea.

Sea	Station	Depth (cm)	MH/DH	MH/HPH	GDGT-0/Cren	Ring Index
Scotia	CTD 1	15	0.5	0.1	2.6	0.9
Scotia	CTD 1	100	0.4	0.2	6.7	0.4
Scotia	CTD 23	20				
Scotia	CTD 23	100	4.7		1.8	0.7
Scotia	CTD 24	15				
Scotia	CTD 24	80	5.3	52.4	1.6	0.9
Scotia	CTD 25	10				
Scotia	CTD 25	80	2.1	0.7	2.4	0.8
Scotia	CTD 22	30				
Scotia	CTD 22	110	2.8	7.7	1.9	0.5
Scotia	CTD 21	30				
Scotia	CTD 21	110	1.1	4.6	5.3	0.2
Scotia	CTD 20	30			2.2	1.0
Scotia	CTD 20	110	1.4	1.3	6.8	0.2
Scotia	CTD 19	20				
Scotia	CTD 19	80	1.1	0.3	8.0	0.3
Scotia	CTD 18	20				
Scotia	CTD 18	90	1.8	0.2	4.1	0.6
Scotia	CTD 16	20				
Scotia	CTD 16	70	5.1	1.0	16.8	1.0
Scotia	CTD 13	30				
Scotia	CTD 13	65		0.5	4.6	0.6
Scotia	CTD 10	30				
Scotia	CTD 10	80		0.2	177.6	0.02
Scotia	CTD 7	40				
Scotia	CTD 7	75		1.1	21.7	0.1
Scotia	CTD 5	20				
Scotia	CTD 5	70	1.1	0.1	4.3	0.7
Scotia	CTD 3	20				
Scotia	CTD 3	60		3.4	9.9	0.3

978

https://doi.org/10.5194/bg-2020-333
Preprint. Discussion started: 5 November 2020

979 Table 6: Ratios of monohexose/dihexose (MH/DH), monohexose/hexosephosphohexose (MH/HPH),

980 GDGT-0/crenarchaeol (GDGT-0/Cren), and Ring Index in the Amundsen Sea.

Sea	Station	Depth (cm)	MH/DH	MH/HPH	GDGT-0/Cren	Ring Index
Amundsen	PS104/003-1	10	0.4	0.0	7.3	0.5
Amundsen	PS104/003-1	120	0.6	0.2	4.8	0.5
Amundsen	PS104/003-1	180	2.2	3.1	27.0	0.03
Amundsen	PS104/003-1	998	0.2	0.4	4.8	0.7
Amundsen	PS104/007-1	20			8.2	0.4
Amundsen	PS104/007-1	120	0.4	0.3	4.9	0.5
Amundsen	PS104/007-1	240	1.5	0.6	5.0	0.4
Amundsen	PS104/007-1	685	0.2	0.2	4.2	0.6
Amundsen	PS104/017-1	10				
Amundsen	PS104/017-1	150	2.8	0.7	5.8	0.3
Amundsen	PS104/017-1	1375	0.1	0.1	2.8	0.9
Amundsen	PS104/022-1	10				
Amundsen	PS104/022-1	30				
Amundsen	PS104/022-1	120	2.8	0.4	3.8	0.6
Amundsen	PS104/022-1	697	0.3	0.4	4.2	0.6
Amundsen	PS104/043-2	10				
Amundsen	PS104/043-2	120	0.3	0.2	3.3	0.5
Amundsen	PS104/043-2	454	0.6	0.1	5.4	0.5

981

982

https://doi.org/10.5194/bg-2020-333
Preprint. Discussion started: 5 November 2020

983 Figure 1. Map showing studied CTD sampling stations (red dots) in the Scotia sea (A) and Amundsen sea
984 (B). The main oceanic fronts are also shown in panel A; subantarctic (SAF), polar (PF), southern ACC
985 (SACCF) and the southern boundary of the ACC (SB) (Sokolov and Rintoul, 2009). The names of the ice
986 shelves are shown in panel B.

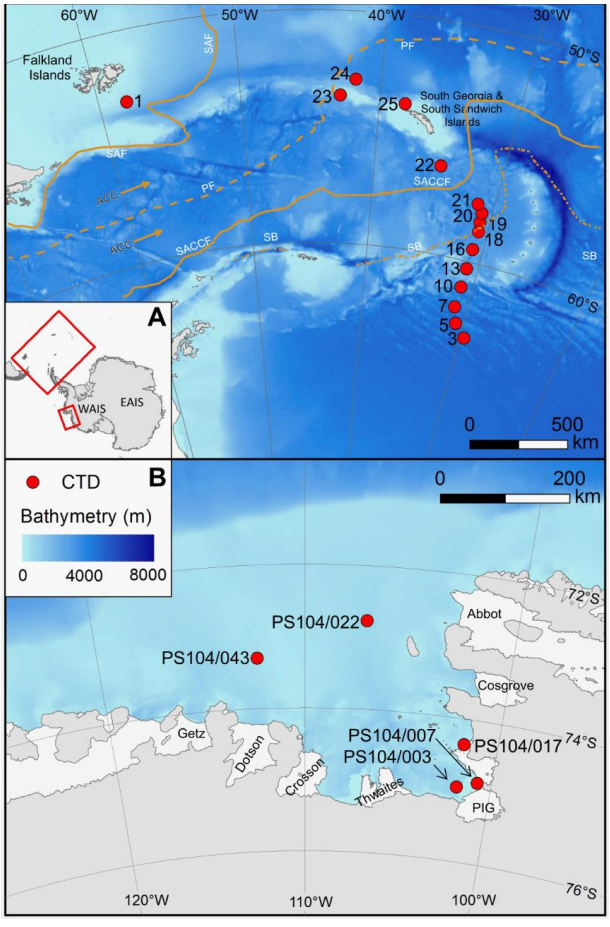

987

https://doi.org/10.5194/bg-2020-333
Preprint. Discussion started: 5 November 2020

988 Figure 2. The Temperature Salinity profiles (T-S plot) for the Amundsen Sea (A) showing Antarctic Surface
989 Water (AASW) and Circumpolar Deep Water (CDW), and Scotia Sea (B). Black dots indicate the CTD data
990 and open triangles indicate the seawater sampling depths.

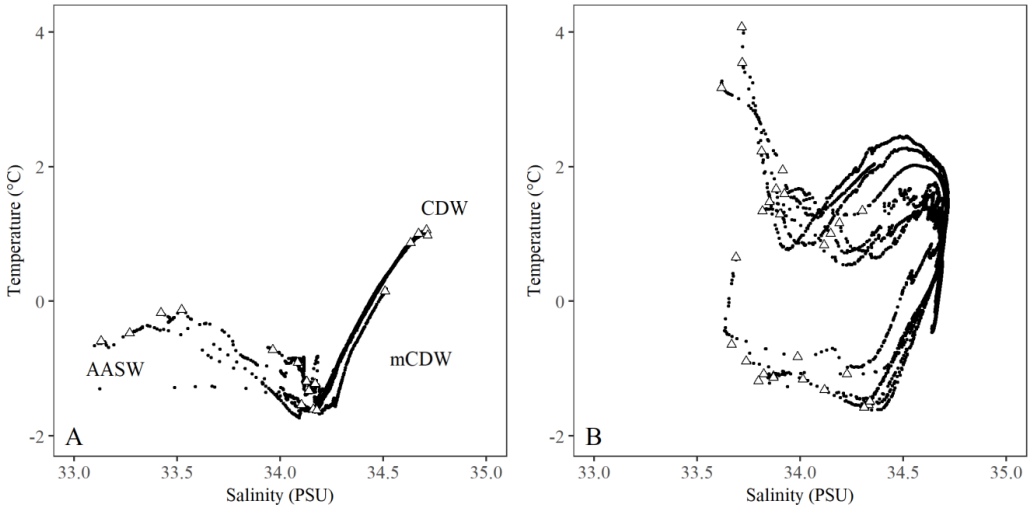

991

https://doi.org/10.5194/bg-2020-333
Preprint. Discussion started: 5 November 2020

992 Figure 3. Total IPL-GDGT concentration (Log_{10}, units/L) (A) and relative abundance (%) of IPL head
993 groups, monohexose (MH, black), dihexose (DH, white), hexose-phosphohexose (HPH, grey) (B) in Scotia
994 Sea thermocline samples (mixed layer samples excluded from plots).

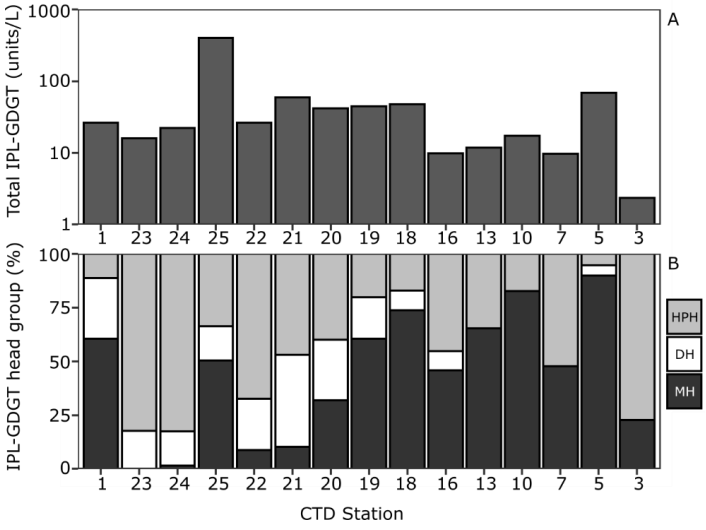

995

https://doi.org/10.5194/bg-2020-333
Preprint. Discussion started: 5 November 2020

996 Figure 4. Relative abundance (%) of intact GDGTs at approximate sample depths in the Amundsen Sea. Bars
997 reflect intact-GDGT head group with black representing MH head groups, white representing DH, and grey
998 representing HPH. Contour lines show approximate ocean temperature ranges using CTD data taken at each
999 sample station with Ocean Data View DIVA gridding.

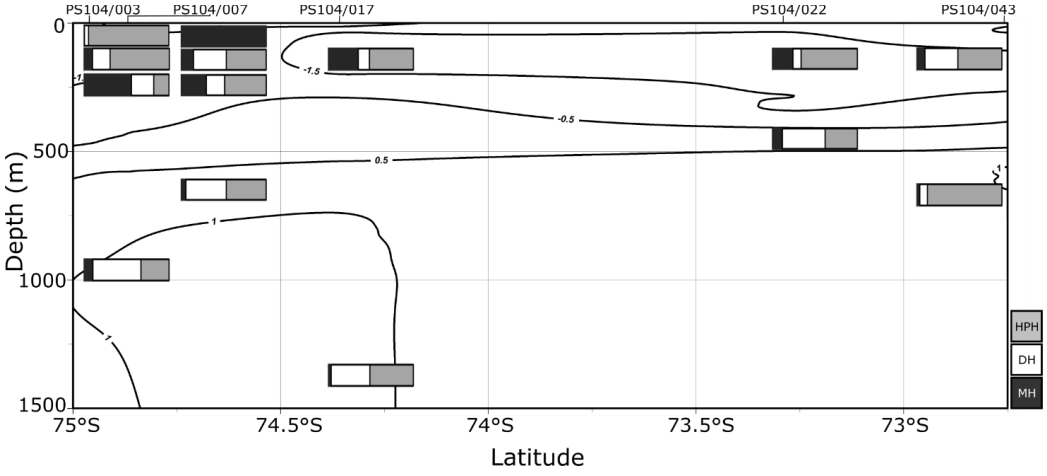

1000

https://doi.org/10.5194/bg-2020-333
Preprint. Discussion started: 5 November 2020

1001 Figure 5. Redundancy analysis triplot for Scotia Sea sample set showing samples with depths, biomarker
1002 response variables (grey lines), and explanatory variables (black with dashed lines indicating statistical
1003 significance).

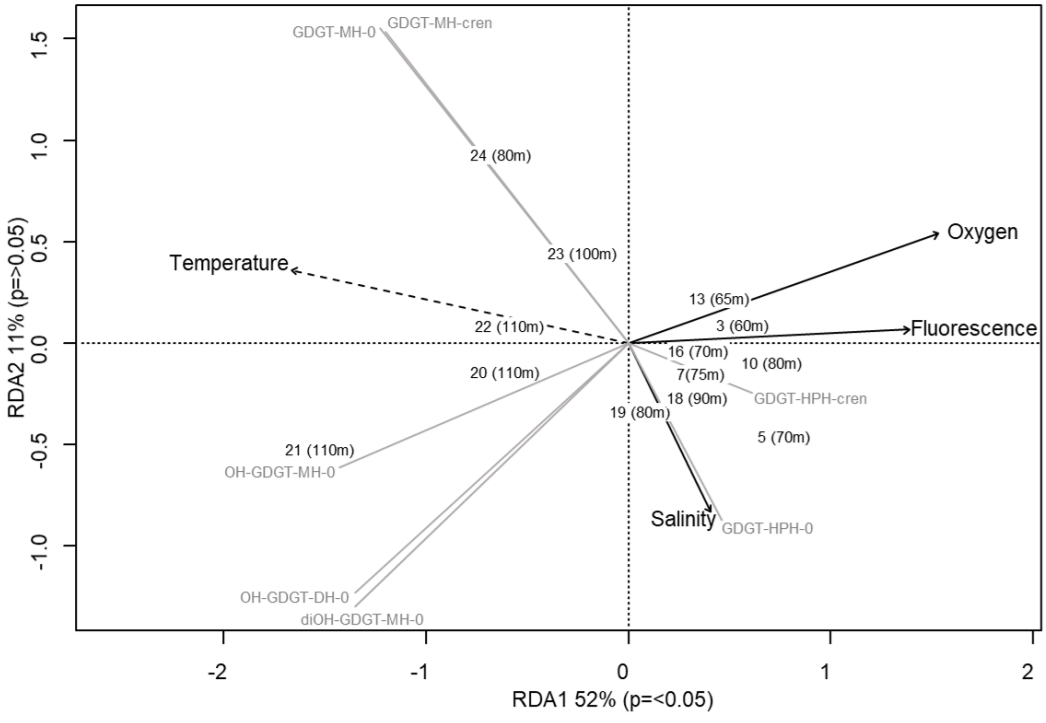

1004

https://doi.org/10.5194/bg-2020-333
Preprint. Discussion started: 5 November 2020


Biogeosciences Discussions Open Access EGU

1005 Supplement A. Absolute masses of IPLS detected in this study including for GDGTs, OH-GDGTs, and
1006 diOH-GDGTs with either MH, DH, or HPH head groups, and for each adduct (H+, NH4+, and Na+).

1007 Supplement B: S1. CTD matrix showing temperature (°C), salinity (PSU), Fluorescence (mg/m^3), Oxygen
1008 (ml/L) for CTD stations PS104/003 (A), PS104/007 (B), PS104/017 (C), PS104/022 (D), PS104/043 (E),
1009 with seawater sample depths indicated by a triangle.
1010 S2. Intact GDGT structures showing GDGT cores where, GDGT: R & R' = H; OH-GDGT: R=OH, R'=H;
1011 diOH-GDGT: R & R' = OH. Monohexose (MH), dihexose (DH), and hexose-phosphohexose (HPH) polar
1012 head groups structures shown.
1013 Supplement C. Redundancy analysis output for Scotia Sea sample set including ANOVA.